Distinct modes of evolution drive HIV escape from two broadly neutralizing antibodies

Elena V. Romero[1,*], Abigail E. Clyde[2,*], Elena E. Giorgi[2], Dylan H. Westfall[2], Walker Azam[2], Megan L. Taylor[1], Marina Caskey[3], Alison F. Feder[1,4,†], Lillian B. Cohn[2,5,†]

[1]Department of Genome Sciences, University of Washington, Seattle, WA, USA
[2]Vaccine and Infectious Diseases Division, Fred Hutchinson Cancer Center, Seattle, WA, USA
[3]Laboratory of Molecular Immunology, The Rockefeller University, New York, NY, USA
[4]Division of Public Health Sciences, Fred Hutch Cancer Center, Seattle, WA, USA
[5]Department of Global Health, University of Washington, Seattle, WA, USA

*These authors contributed equally to this work
[†]These authors co-supervised this work; to whom correspondence should be addressed:
lcohn@fredhutch.org, affeder@uw.edu

Abstract

Broadly neutralizing antibodies (bNAbs) show promise for HIV treatment and prevention, but are vulnerable to resistance evolution. Comprehensively understanding *in vivo* viral escape from individual bNAbs is necessary to design bNAb combinations that will provide durable responses. We characterize viral escape from two such bNAbs, 10-1074 and 3BNC117, using deep, longitudinal sequencing of full length HIV envelope (*env*) genes from study participants treated with bNAb monotherapy. Improved sequencing depth and computational evolutionary analyses permit us to identify *in vivo* routes and parallelism underlying HIV escape from each bNAb, providing new insights into this evolutionary process: 10-1074 escape is restricted to a small number of previously documented pathways, but these escape mutations 1) pre-exist in intra-host viral populations before therapy, 2) are not all equally preferred, and 3) emerge with a high degree of genetic parallelism within and across viral populations. In contrast, 3BNC117 escape follows background-specific patterns in which specific escape mutations present in one population rarely emerge or spread in other populations, but often still exhibit parallel evolutionary responses within their host. That bNAbs elicit starkly different *in vivo* escape profiles depending on their Env target exposes the limitations of generalizing escape patterns across therapies and highlights the substantial challenges in predicting a viral population's bNAb susceptibility from genetic diversity alone.

Significance Statement

Analyses of HIV clinical trial data have long been limited by tradeoffs between sequencing at high depth and preserving genetic linkage information. Using recently developed techniques eliminating this trade off, we deeply re-sequenced samples from two clinical trials of broadly neutralizing antibody (bNAb) monotherapies. We employed novel and established computational analyses to characterize HIV populations with unprecedented resolution as they escaped these therapies. Tracking single escape mutations in the context of their genetic backgrounds, we find starkly different patterns of escape from these two bNAbs with distinct target regions, 10-1074 and 3BNC117. Our findings highlight the difficulties in evaluating pre-treatment resistance; thus, careful antibody selection for future studies will be needed to maximize the likelihood of durable efficacy.

Introduction

Combination antiretroviral therapy (cART) has revolutionized the treatment and prevention of HIV-1 infection. However, cART does not eradicate established infection (Chun et al., 1997; Cohn et al., 2020) and worldwide HIV-1 incidence rates remain high (UNAIDS Data 2024 | UNAIDS, 2024). Thus, the search for novel preventive and therapeutic interventions remains a global high priority. Broadly neutralizing antibodies (bNAbs) have emerged as a possible new therapeutic and preventive strategy because antibodies allow for infrequent dosing, directly target multiple viral epitopes, and have the potential to harness host immune responses via their Fc effector domains (Bournazos et al., 2017). However, their clinical development has been hindered in part because bNAbs are vulnerable to escape by HIV-1 variants.

In vivo, HIV rapidly escapes bNAb monotherapies through the generation of resistance (i.e. escape) mutations (Caskey et al., 2015, 2017; Lynch et al., 2015; Stephenson et al., 2021). However, combining bNAbs into co-administered cocktails has begun to yield promising results (Eron et al., 2024; Gaebler et al., 2022; Julg et al., 2024), mirroring the therapeutic development of cART cocktails in the 1990s. Different bNAbs target different sites of the HIV Env protein spike, including the CD4 binding site (CD4bs), the V1V2-glycan epitope, the V3-loop region, gp120-gp41 interface and the membrane-proximal external region (MPER). Multiple bNAbs applied simultaneously thus challenge the virus combinatorially, raising the genetic barrier to full resistance (Julg et al., 2024; Mahomed et al., 2022; Mendoza et al., 2018; Sneller et al., 2022; Mayer et al., 2022; Wagh et al., 2016). Recent work has shown that viral escape from pooled antibodies can be well described by investigating the action of each antibody component independently then employing an additive model of their effects (Dingens et al., 2019; Yu et al., 2022). Realizing combination bNAb therapy's potential as a long-term treatment, prevention, and possibly even cure, of HIV will likely therefore rely on comprehensively characterizing viral escape from individual bNAbs to design optimal combinations (LaMont et al., 2022).

First, the diversity of viral escape routes from individual bNAbs is still incompletely understood. *In vitro* approaches like deep mutational scanning (DMS) and neutralization experiments permit the systematic characterization of viral escape phenotypes against specific bNAbs (Bricault et al., 2019; Dingens et al., 2019; LaBranche et al., 2018; Radford & Bloom, 2025; Schommers et al., 2020). Nevertheless, it remains unclear if these represent the full range of escape trajectories achieved *in vivo* and how these results generalize to new viral genetic backgrounds. For example, Radford et al. recently found that two divergent envelope strains from different subtypes achieved 3BNC117 escape via different mutations, suggesting that escape may be dependent on the genotypic context in which it arises (Radford & Bloom, 2025). In the more complex situation of people living with HIV who harbor widely divergent HIV variants, it is still unclear how often diverse viruses evolve the same strategies to escape bNAbs. Profiling escape mutations *ex vivo* in diverse HIV populations treated with bNAbs can reveal if and when escape depends on genetic background and uncover escape-associated genetic variation like indels not generally evaluated in DMS experiments.

Second, a deeper understanding of how often single intra-host populations produce escape variants *in vivo* (i.e., the degree of evolutionary parallelism) can provide insight into the simultaneous challenges necessary to durably suppress HIV. Here, we define evolutionary parallelism as multiple viruses acquiring similar characteristics (i.e., antibody escape) while evolving together at the same time (*Parallel Evolution - an Overview*, n.d.). A high degree of evolutionary parallelism generally indicates that mutations conferring escape are readily available to a population, either as standing genetic variation that pre-exists before therapy or via *de novo* mutation occurring after therapy onset. Parallelism can emerge because many different mutations confer escape, genomes mutate at a high rate, and/or because the population size of those viruses that can produce the mutations is large. Recognition of parallelism driving escape from ART monotherapy helped scientists establish that multiple distinct therapies needed to be combined to effectively limit viral populations'

access to fully-resistant escape profiles. Similarly, profiling parallel evolution during bNAb escape could improve estimates of how many components would be needed for combination therapies to achieve durable suppression. Previous bNAb monotherapy studies have observed that intra-host viral populations also appear to escape via multiple mutations concurrently (Caskey et al., 2015, 2017; Williamson et al., 2025) and theoretical predictions based on the number of mutationally accessible genotypes support these observations (LaMont et al., 2022). However, the full extent of this parallelism has not been investigated *in vivo*.

We therefore sought to understand the *in vivo* routes and parallelism of HIV escape from two broadly neutralizing antibodies, 10-1074 and 3BNC117, which target the V3 glycan and CD4 binding site, respectively. Previous attempts to address these questions have been constrained by limited sequencing depth using conventional single genome analysis methods (Caskey et al., 2015, 2017; Schoofs et al., 2016). While deep sequencing approaches can characterize *in vivo* viral evolution with high resolution, they rely on short reads where information about viral genetic background is lost (Caskey et al., 2017; Zanini et al., 2015). We therefore leveraged a novel high throughput, long-read strategy to sequence longitudinal plasma samples from two bNAb monotherapy clinical trials of 10-1074 and 3BNC117. This approach, called SMRT-UMI, permitted substantially deeper sequencing than previously employed single genome amplification approaches (~10-100x) while also retaining critical information about the genetic backgrounds on which resistance mutations occur (Westfall et al., 2024). For both bNAbs, high-resolution haplotype analysis revealed new insights into therapeutic escape.

Results

High resolution sequencing yields fully resolved *env* haplotypes.

To collect high resolution, linkage-resolved sequences from viral populations escaping bNAbs, we adapted a long-read, high throughput, deep sequencing method (SMRT-UMI) to sequence full-length HIV envelope (Fig. 1a) (Westfall et al., 2024). Briefly, a unique molecular identifier (UMI) is attached to viral cDNA prior to amplification. We then perform PCR to amplify HIV envelope and use a long-read sequencing approach to capture the full-length HIV *env* gene and its linked UMI. Using this method, we sequenced HIV *env* from 20 donors using plasma samples from clinical trials NCT 02511990, which involved a single administration of 10-1074 to viremic participants living with HIV (PLWH), and NCT 02018510, which involved a single administration of 3BNC117 to viremic PLWH, (Fig. 1b) (Caskey et al., 2015, 2017). Treatment with 10-1074 reduced plasma viremia by 1–3 logs in 9 of 11 participants, and 3BNC117 treatment had similar effects in 8 of 9 participants. However, viral loads rebounded to pre-treatment levels by weeks 4-12, driven by both declining antibody concentrations and the emergence of resistant variants. Samples were collected at day 0, week 1, and week 4 after antibody administration, and at later time points in a subset of individuals (Fig. 1d, Supp. Tables 1,2 for full sampling scheme).

In total, we recovered 2324 *env* sequences from 11 study participants treated with 10-1074 (median 40; range: 1-198), and 4405 full length *env* sequences from 9 study participants treated with 3BNC117, including one transmission pair, (median 68; range: 4-373), all of which were Clade B (Fig. 1c). Two timepoints (2E5 week 1 and week 4, 17 sequences) were sequenced using conventional single genome sequencing methods due to low viral loads and limited previously reported data (Caskey et al., 2015). This sequencing effort represents 3.5x (2324/657) - 7.5x (4388/575) increase in depth above the original conventional single genome sequencing studies for 10-1074 and 3BNC117, respectively (Caskey et al., 2015, 2017; Schoofs et al., 2016). In phylogenetic analyses, these sequences clustered by participant, confirming the absence of donor-to-donor contamination using the SMRT-UMI method and filtering approach (Supp. Fig. 1, 2). Recovery of sequences

varied by participant and correlated with viral load (Fig. 1d; 10-1074 Spearman $\rho = 0.784$, $p = 1.352 \times 10^{-6}$; 3BNC117 $\rho = 0.685$, $p = 7.90 \times 10^{-7}$).
For downstream analyses, we aligned the filtered sequences by participant along with previously recovered SGA sequences (Supp. Tables 3,4, Caskey et al., 2015, 2017; Schoofs et al., 2016).

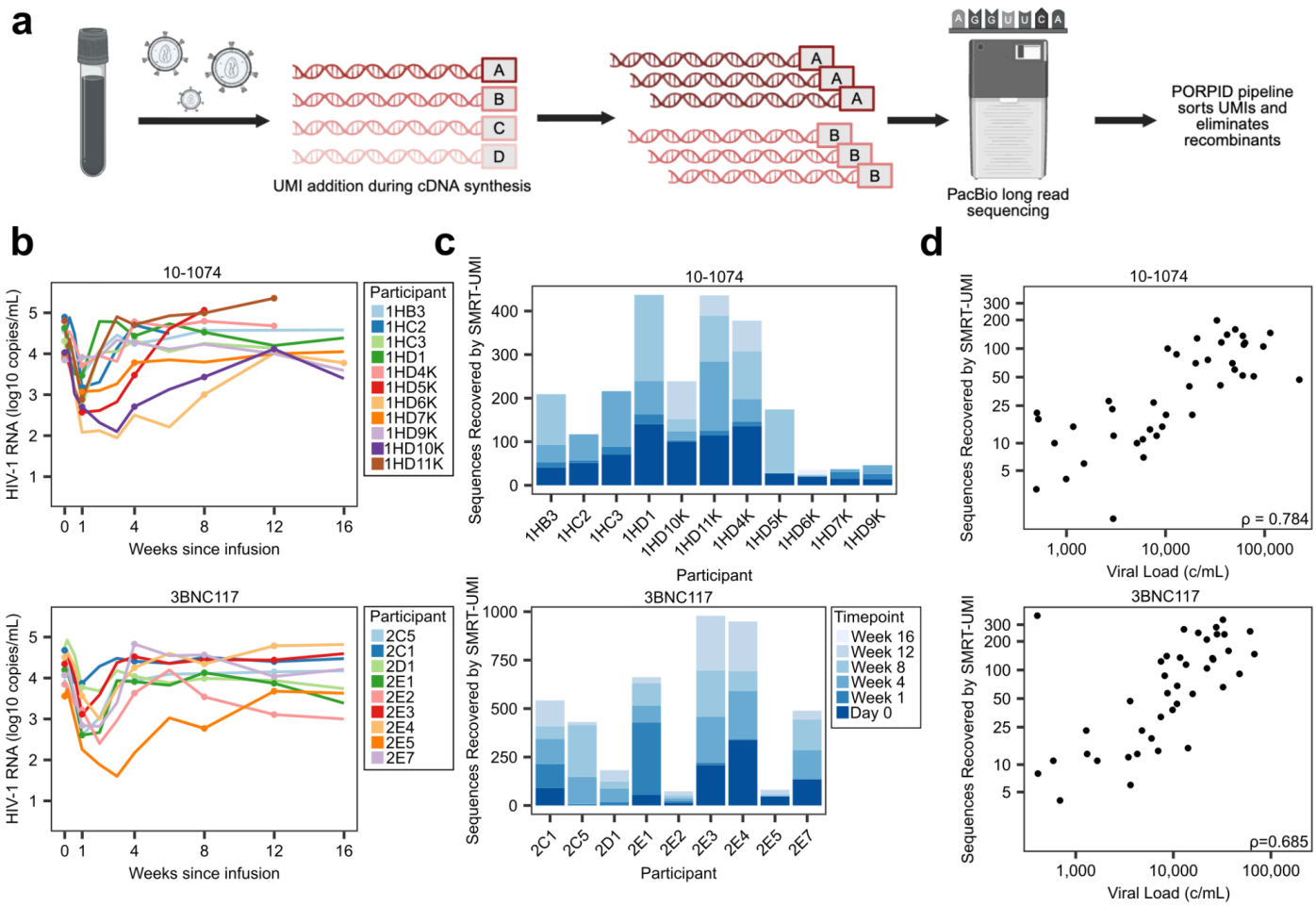

Figure 1: High-resolution sequence recovery of samples from human clinical trials testing two broadly neutralizing antibody monotherapies infused during chronic HIV infection. (**a**) Schematic representation of SMRT-UMI sequencing protocol. (**b**) Viral load graphs following 10-1074 (top) or 3BNC117 (bottom) infusion from NCT 02511990 and NCT 02018510, respectively. Each color represents a participant and dots indicate timepoints sequenced (see Supp. Tables 1,2 for complete sampling scheme) (**c**) Number of sequences recovered per participant using SMRT-UMI, separated by time point. Sequences recovered in 10-1074 treated samples (top) and 3BNC117 treated samples (bottom). (**d**) The number of sequences recovered using SMRT-UMI is positively correlated with viral load (copies/mL) in the 10-1074 treated samples (top) and 3BNC117 treated samples (bottom). Spearman $\rho = 0.784$, $p = 1.352 \times 10^{-6}$ (top); $\rho = 0.685$, $p = 7.90 \times 10^{-7}$(bottom).

Viruses escaping 10-1074 follow well-described pathways but also exhibit changes in variable loop content.

We first investigated HIV amino acid (AA) sequence changes following 10-1074 infusion to assess the full range of escape pathways observed during the trial. We identified variable loci in 10-1074 treated participants where the day 0 consensus AA decreased by at least 40% in frequency after bNAb administration (see

Materials & Methods). In concordance with previous shallower single genome sequencing results (Caskey et al., 2017), we identified large and consistent AA changes at loci N332, S334 and D/N325 after 10-1074 infusion which partially reverted in some participants by the end of the trial, potentially indicative of a fitness cost of escape (Fig. 2a-d, Supp. Fig. 3, Supp. Table 5). As expected, these mutations had high antibody escape scores in a recent deep mutational scan (DMS) of HIV escape from 10-1074 (Supp. Fig. 4, Radford & Bloom, 2025). Mutations at N332 and S334 responsible for the removal of the N332 glycan did not appear to depend on the genetic background of the virus. The one exception was participant 1HD9K whose HIV population had a pre-existing escape mutation at another 10-1074 contact site, D/N325E, potentially lessening the selective benefit of N332 glycan loss.

To look for additional putative escape mutations, we identified all loci that showed $\geq 40\%$ day 0 consensus AA loss across 3 or more participants (Supp. Table 5). In addition to the loci described above, V4 locus 406 also showed AA changes in 4 individuals, although the locus may not be comparable across all individuals due to alignment challenges in this hypervariable region (Supp. Table 5, Supp. Fig. 5). While locus 406 has not been previously associated with 10-1074 resistance, DMS linked locus 406 to escape from PGT121, another V3-targeting bNAb (Dingens et al., 2019). Several other loci in V4 and V5 also passed our consensus loss filtering criterion in multiple individuals (Supp. Table 5). However, due to their hypervariability, we instead examined changes in the length and number of glycosylation sites in the variable loop regions. The loss of N332 glycan in V3 was the only change that was widely shared (10/10 participants without pre-existing high frequency resistance), but multiple other variable loop length and glycosylation patterns changed over time which might be linked to 10-1074 resistance (Supp. Fig. 6,7, Bai et al., 2024; Bricault et al., 2019; Zacharopoulou et al., 2024).

We therefore conclude that while loss of the N332 glycan and mutations at locus 325 appear to be the primary drivers of 10-1074 escape, other changes may also play a role.

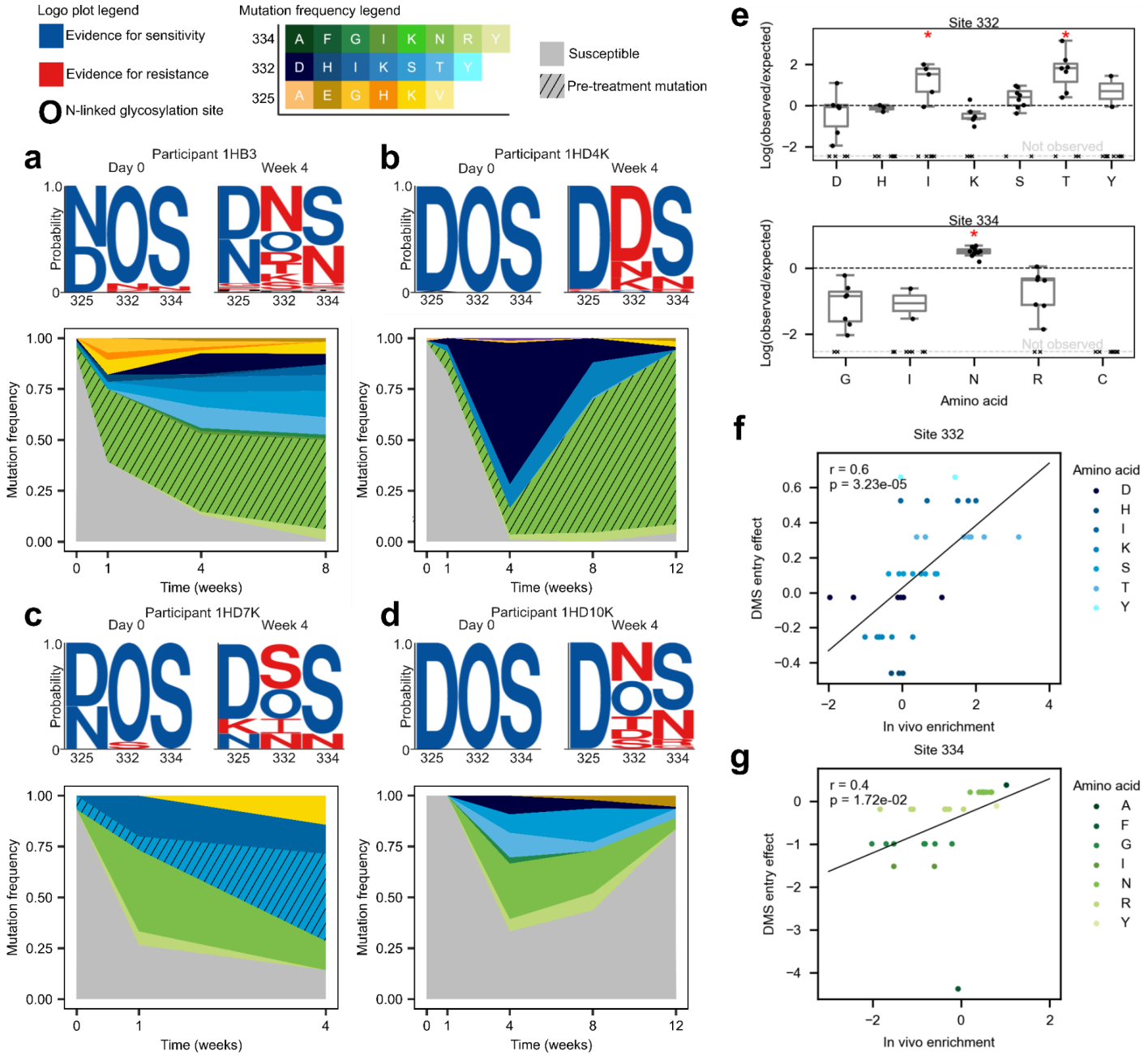

Figure 2. Dynamics and relative enrichments of viral escape mutations following 10-1074 treatment. **(a-d)** (top) Logo plots of amino acids (AAs) at loci 325, 332, and 334 are shown for pre-treatment time point (day 0) and the first post-nadir time point (week 4) in select 10-1074 treated participants. AAs in red or blue have previously been reported to confer resistance or sensitivity to 10-1074, respectively (Bricault et al., 2019; Caskey et al., 2017; Dingens et al., 2019; Radford & Bloom, 2025). (bottom) Frequency plots of escape mutations over time are shown, with each mutation indicated by color and hatching indicating those escape mutations discovered pre-treatment. Additional participants are shown in supplemental figure 3. **(e)** Observed mutational frequencies in the trial data were compared to predicted mutational frequencies calculated based on the probability of the day 0 ancestral codon mutating to a given AA (See Materials & Methods) at loci 332 & 334. Ratios of log(Observed/Expected) > 0 indicate an enrichment above neutral expectation. Each data point represents the comparison for a single participant. Hatch marks on the "Not observed" line indicate participants in which the change was expected by mutation, but not observed. Significance was determined via binomial tests with a Bonferroni correction (significance level $\alpha = 3.1 \times 10^{-3}$, $p = 6.6 \times 10^{-9}, 1.2 \times 10^{-4}, 7.5 \times 10^{-35}$ for N332T, N332I, and S334N, respectively). **(f,g)** *In vivo* enrichment,

log(Observed/Expected), for each AA sampled in each participant, plotted against cell entry effects for TZM-bl cells as determined by deep mutational scanning of the clade B TRO11 HIV Env protein (Radford & Bloom, 2025) for sites 332 and 334. Pearson $r = 0.6$, $p = 3.2 \times 10^{-5}$ (site 332); $r = 0.4$, $p = 1.72 \times 10^{-2}$ (site 334).

10-1074 escape pathways appear to be shaped by functional conservation.

We next investigated the factors underlying which specific AA substitutions drove glycan loss at N332, the primary identified driver of 10-1074 escape. We first hypothesized that low frequency pre-existing escape mutations may become the most prevalent escape mutations following bNAb infusion. Our deeper sequencing revealed three 10-1074 participants with pre-existing escape motifs at N332 on day 0 (1HB3, 1HD4K, 1HD7K), which persisted through the study period (Fig. 2a, c, e). However, pre-existing escape mutations were not associated with rebound timing or viral loads at weeks 0 or 1, after removing one outlier with pre-existing escape mutations at 100% frequency (Supp. Fig. 8). Furthermore, those pre-existing mutations did not dominate sequences recovered at later time points (for example, S334N in 1HD4K, Fig. 2b). A potential explanation for this pattern is that many escape mutations pre-exist below our detection limit or can easily be produced by mutation, such that escape mutations sampled at day 0 do not have an appreciable advantage over others.

We next hypothesized that the most prevalent escape AAs might be those most easily generated via mutation. To test this hypothesis, we calculated the relative probabilities of generating each escape AA at sites 332 and 334, assuming equivalent fitness benefits, based on participant-specific ancestral codons and previously estimated mutation rates (Zanini et al., 2017). We then compared the relative probability of generating each escape AA to its observed frequency *in vivo* (Supp. Fig. 9) and found that N332T, N332I, and S334N were significantly enriched *in vivo* after 10-1074 administration compared to their probability of being generated by mutation (Fig. 2e, Binomial tests, $\alpha = 3.1 \times 10^{-3}$, $p = 6.6 \times 10^{-9}$, 1.2×10^{-4}, 7.5×10^{-35}, respectively). We further found a positive correlation between how favored an escape AA was *in vivo* and its effects on viral cell entry capability as measured via DMS (Site 332: Fig. 2f. Pearson $r = 0.6$ & $p = 3.2 \times 10^{-5}$, Site 334: Fig. 2g $r = 0.4$ & $p = 1.7 \times 10^{-2}$, TRO11 clade-matched DMS backbone), although we note that some DMS results can be backbone-dependent (Haddox et al., 2018). We additionally note that S334N caused a 332 to 334 glycan shift in two participants (1HD4K & 1HD5K). Therefore, while many mutations can remove the N332 glycosylation site, additional selective forces, including glycosylation shifting and cell entry capability, may shape their observed frequencies *in vivo*.

Distinct lineages within each participant follow the same 10-1074 escape pathways.

Both our findings and those of Caskey et al. 2017 indicate that 10-1074 escape is driven by multiple distinct AA changes spreading in parallel within single intra-host viral populations (Caskey et al., 2017). Using deeper sequencing and linkage information, we tested for additional cryptic origins of resistance in which multiple different viruses within a single intra-host viral population escaped via the exact same AA change.

We first examined how often distinct nucleotide substitutions generated the same AA change following 10-1074 administration, indicating multiple mutational origins. Among escape AAs with multiple possible codon encodings accessible from an ancestral AA via a single nucleotide change, the majority (14/24) were encoded in multiple ways within single participants, indicating that more than one nucleotide substitution had occurred.

Three distinct nucleotide substitutions could generate S334R, and one participant's viral population, 1HD11K, contained all three of them (Fig. 3a). In contrast, no newly appearing AAs at loci other than 325, 332, or 334 were multiply encoded, even when reaching relatively high frequencies, suggesting this characteristic was restricted to loci under strong selection.

Because not all AAs that confer resistance can be multiply encoded, we further examined if the exact same escape mutation could be observed in tight genetic linkage to multiple viral backbones harboring different nearby mutations. We examined 150bp flanking either side of the escape motif (i.e., sites 325-334) and matched each unique post-treatment sequence to its closest ancestors at any previous time point (Fig. 3b-g, Supp. Fig. 10).

This analysis revealed two primary conclusions about parallel evolution in response to 10-1074. First, the same pre-treatment genetic background is often rescued by multiple distinct escape mutations (Fig. 3h,i, Supp. Fig. 11). Sequences which were identical at day 0 often appeared at later time points with different escape mutations, but no other changes in the flanking regions (for example, Fig. 3b,c,e,f). Second, the same escape mutations often emerge in parallel on distinct genetic backgrounds. We observed these patterns in all responding participants except 1HD7K, from whom only 6 sequences were recovered at week 4. We further found that escape mutations arose on significantly more genetic backgrounds than non-escape mutations (Fig. 3j, Multiple linear regression, interaction coefficient for allele frequency and escape status: $\beta_{Allele\ Frequency:Non-escape} = -20.28, p = 1.03 \times 10^{-77}$). Although rapid recombination can move escape mutations between genetic backgrounds, tightly conserved linkage structure on both sides of the escape motif suggest that at least some of these instances represent additional instances of independent mutational origins of therapeutic resistance (Fig. 3b,c,e,f).

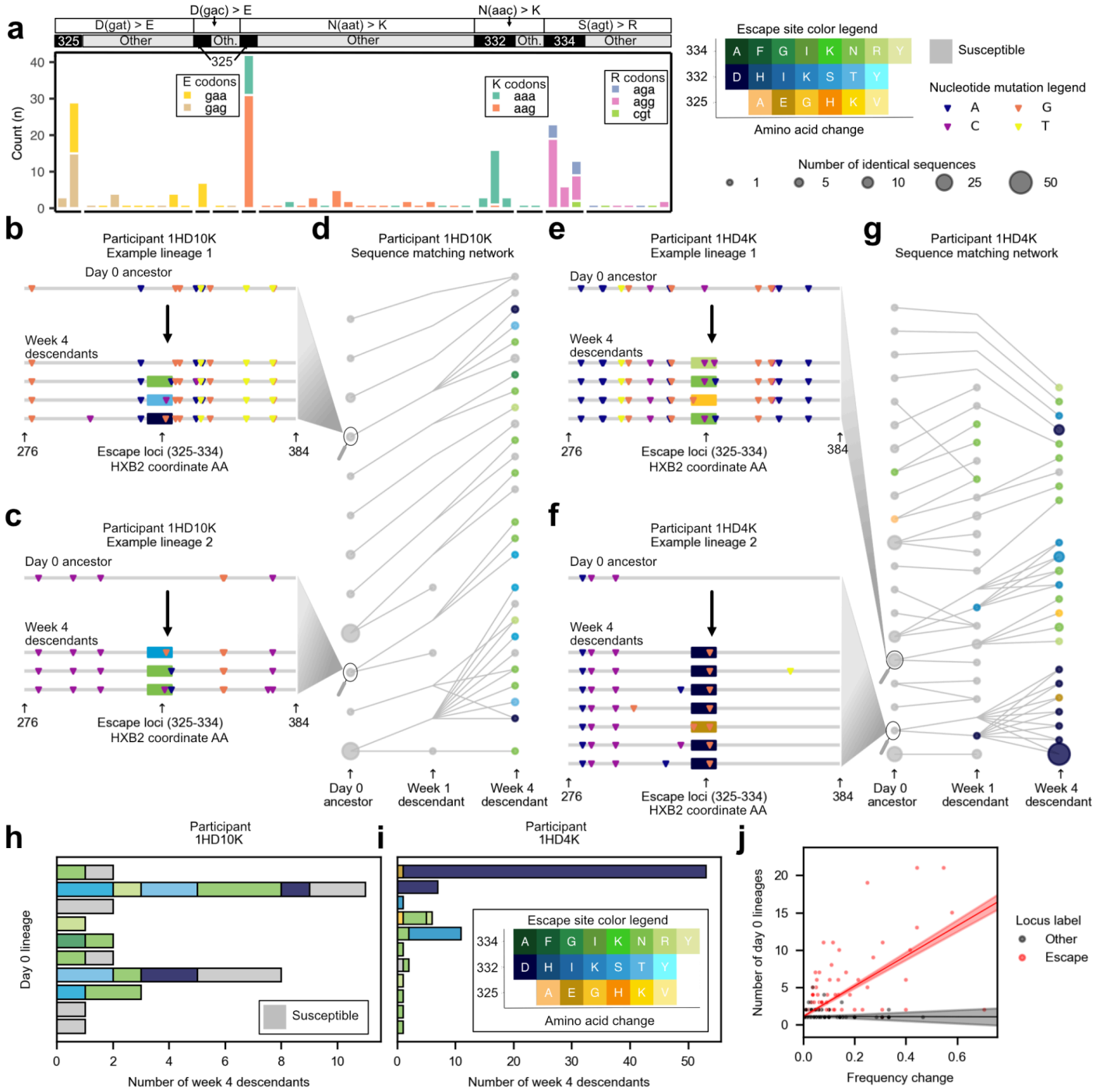

Figure 3. Escape from 10-1074 is highly parallel, with multiple occurrences of the same AA change spreading concurrently within participants.

(a) Nucleotide codon encodings for AAs appearing after 10-1074 treatment stratified by ancestral AA nucleotide encoding. Each stacked bar represents nucleotide encodings for a single AA at a given locus from a single participant at an escape locus (325, 332, 334) or a non-escape locus (other). **(b-g)** Haplotype windows of 150bp flanking the 10-1074 resistance region were traced back to their common ancestors and matched via minimum Hamming distance in participants 1HD10K & 1HD4K. Highlighter plots (b,c,e,f) show haplotype examples of descendant-ancestor pairs. Network plots (d & g) indicate the descendant-ancestor relationships (edges) between sequences (nodes) at different timepoints. Sequences are connected to all equidistant ancestors. Sequences with multiple escape mutations are colored based on the escape mutation with the lowest HXB2 coordinate (applicable to panel f only). Haplotype networks for other participants are

shown in supplemental figure 10. **(h-i)** Bar plots of escape mutations carried by week 4 descendants of each day 0 lineage. Additional participants are shown in supplemental figure 11. **(j)** Number of day 0 lineages carrying each escape-associated (red) or non-escape-associated (grey) AA as a function of the AA's maximum frequency increase during the trial. Escape-association was a significant predictor of the lineage count (Multiple linear regression, interaction coefficient for allele frequency and escape status: $\beta_{AA\ Frequency:Non-escape} = -\ 20.28, p = \ 1.03\ \times 10^{-77}$)

Viral populations treated with 3BNC117 develop mutations at diverse loci

We next sought to identify mutations associated with 3BNC117 escape by identifying AA changes following bNAb administration in the 3BNC117-treated cohort. Unlike in the 10-1074 treated individuals, no loci showed consistent AA changes between pre- and post-treatment timepoints across the majority of individuals receiving 3BNC117 (see Materials & Methods, Supp. Table 6), although all study participants experienced a dip and rebound in viral load. To detect participant-specific AA changes associated with escape, we conducted a selection scan using Marginal Path Likelihood (MPL), a method to identify positively selected loci from longitudinally sampled haplotype data (Sohail et al., 2021), and supplementary approaches to detect subtle 3BNC117-driven evolution not readily detectable by MPL.

MPL identified 11 loci under strong positive selection across seven different participants (Supp. Table 7, Supp. Fig. 12). These sites exhibited selection coefficients high enough ($s \geq 0.044$) to drive a substantial AA frequency increase during the trial (predicted to reach or exceed 15% frequency from a starting frequency of 5%, see Materials & Methods). In contrast to the convergent escape pathways observed for 10-1074, where participants developed similar mutations, responses to 3BNC117 were more heterogeneous, with only changes at locus 282 and in an insertion near locus 459 shared across two participants. (Fig. 4a). The majority of the identified loci (6/11) have either been previously linked to 3BNC117 escape (Bricault et al., 2019; Dingens et al., 2019; LaBranche et al., 2018; Radford & Bloom, 2025; Scheid et al., 2016; Schommers et al., 2020) or fall in 3BNC117 contact sites (Schoofs et al., 2016; Zhou et al., 2013). In two participants, 2C1 and 2E1, MPL did not identify any loci under strong positive selection (Supp. Fig. 12).

MPL identifies the loci most likely to be under positive selection in the context of their genetic background, but cannot always disambiguate selected versus hitchhiking mutations when those loci are highly genetically linked. We therefore also ran MPL treating each locus independently and found 9 additional loci in 3BNC117 contact domains that passed our filtering threshold ($s \geq 0.044$). In all participants except 2E1, these additional loci were all highly genetically linked ($D' \geq 0.69$) to another selected variant, suggesting that mutations at these sites could be hitchhiking or interacting epistatically. We report these loci in supplemental table 8 and in figure 4a as "additional variation," but conservatively do not include them in subsequent analyses unless otherwise noted.

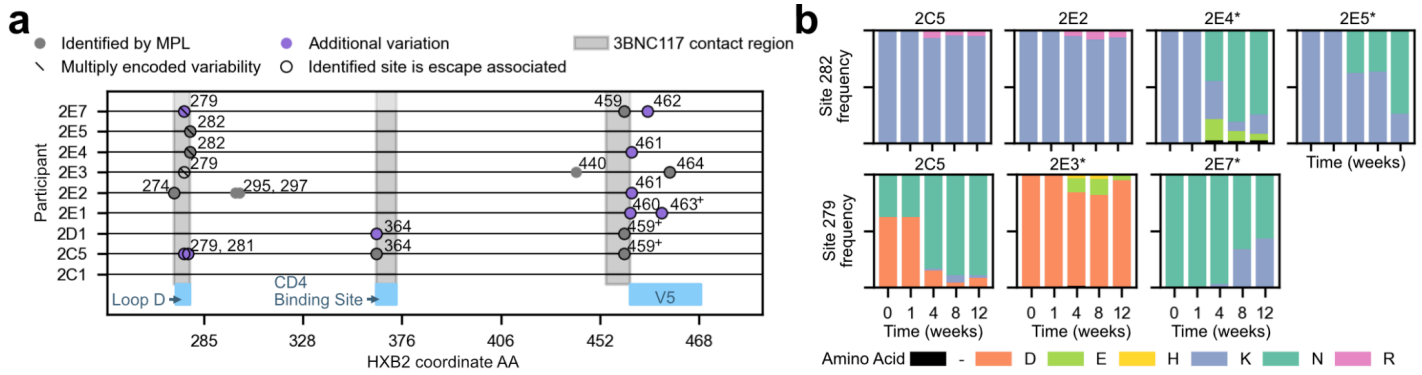

Figure 4. Loci changing following 3BNC117 administration exhibit only modest conservation across participants at the locus level and limited conservation at the AA level. **(a)** Putative escape loci against 3BNC117 identified in different participants (see Materials & Methods). Stacked symbols indicate that a locus was identified via multiple approaches. Black circular outlines denote loci with literature support (Bricault et al., 2019; Dingens et al., 2019; LaBranche et al., 2018; Radford & Bloom, 2025; Schommers et al., 2020) or those falling in 3BNC117 contact regions (Schoofs et al., 2016; Zhou et al., 2013). Five loci without literature support outside of the contact regions (HXB2 coords 90, 97, 145, 706, and 754 in participants 2D1, 2E2, 2C5, 2E1, and 2E7, respectively) are not plotted (see supplemental tables 7 and 8 for all identified loci). $^{+}$denotes variation in an insertion relative to HXB2 at the listed coordinate. **(b)** Bar graphs of AA frequencies at escape loci identified in at least two participants. All participants with variation at each locus are shown, and * denotes participants where the locus was identified by a selection scan.

Our 10-1074 analysis revealed that newly observed AAs encoded by multiple nucleotide triplets can also indicate positive selection (Fig. 3a), so we repeated the multiple encoding analysis using data from the 3BNC117 cohort and found four additional loci with evidence for positive selection: locus 279 in two participants (2E3 and 2E7) and loci 97,145, & 706 in participants 2E2, 2C5, and 2E1, respectively (Fig. 4a). In addition, we discovered that mutations at locus 282 were multiply encoded in 2E4 and 2E5, corroborating their identification by MPL. Of these loci, previous studies have linked mutations at 279 and 282 to 3BNC117 escape (Bricault et al., 2019; Schommers et al., 2020) while locus 97 has been linked to escape for other bNAbs targeting the CD4 binding site (Chen et al., 2021; Dingens et al., 2019; Huang et al., 2016).

In total, we identified loci under strong positive selection in 8/9 participants (excluding 2C1). Supplemental table 7 and figure 4a show loci identified by our selection scans (MPL or multiple-encoding analysis).

While our findings were broadly concordant with the original single genome sequencing studies (Caskey et al., 2015; Schoofs et al., 2016), increased sequencing depth enabled more accurate measurement of AA frequency trajectories in key regions (Supp. Fig. 13-21). For example, in the original data, participant 2E3 had variation in loop D only 12 weeks after 3BNC117 infusion and at low frequency (D279E and D279H in 3/24 sequences, Caskey et al., 2015). However, deeper and more extensive sequencing revealed that these mutations circulated consistently from weeks 4 through 12 with a maximum frequency of 18% at week 8 (Supp. Fig. 18). Conversely, mutation 459E in participant 2D1 appeared fixed by week 4 in the original data, but deeper sequencing revealed that it remained below 27% frequency throughout the trial (Supp. Fig. 15).

In addition to clarifying the trajectories of previously identified mutations, we also found 11 AA identities in 5 participants at sites under strong positive selection which were not identified in the original sequencing studies, (Supp. Table 9, Caskey et al., 2015; Schoofs et al., 2016). Many of these newly identified AAs (9/11) remained

at low frequencies (<10%) but circulated at multiple timepoints. Together, these findings suggest that deeper sequencing enhances our ability to detect viral diversity and selection responses after bNAb infusion.

V5 changes were common after 3BNC117 infusion, but not concordant across participants

V5 is a known contact region for 3BNC117 and thus a likely site of viral escape; however, its high variability makes direct comparison of specific loci across participants challenging. Therefore, we examined non-single nucleotide variant (SNV) based variation in V5 in the form of loop length and potential N-linked glycosylation (PNG) shifts and losses. In all participants, we found minimal changes in the V5 variable loop length and only two participants had minor decreases in the total number of V5 PNGs (2C5, 2E7, Supp. Fig. 22,23).

However, the location of V5 PNGs often shifted during the trial, displaying >10% frequency shifts in all participants except 2E3, 2E4 and 2E5 (Supp. Fig. 24, see Materials & Methods). These shifts occurred between PNGs at loci 460, 462, 463 and 465, although they did not show consistent directionality. Their magnitude was above 25% in participants 2C5, 2D1, 2E1, and 2E7 (Supp. Fig. 24). In 2C5, 2D1 and 2E7, these large shifts also corresponded to a SNV trajectory identified by our selection scans as under positive selection. These findings confirm that the V5 terminal region is important in 3BNC117 escape, but their heterogeneity across participants further suggests that specific motifs related to escape are highly dependent on the genetic context of the viral strain.

Escape AA identities can be participant-specific even when escape loci are shared across participants.

Although the escape loci identified by our selection scans in the 3BNC117-treated cohort were less concordant than those identified in the 10-1074-treated cohort, we observed some degree of sharing at loci 279, 282, and the V5 region loci (including 459-463) characterized above. To determine if loci 279 and 282 escaped via shared or participant-specific AA identities, we plotted the distributions of AAs at these loci over the course of the trial (Fig. 4b). We included all participants with variation at each of these loci, even those not directly detected in our selection scans.

Locus-specific concordance in AA responses across participants depended on pre-infusion AA similarity. At locus 282, all four participants with variation during the trial started with K282 at 100% frequency prior to treatment. Both participants with MPL-identified positive selection at this locus (2E2 and 2C5) showed similar large increases in K282R, while the two participants without MPL-identified positive selection experienced smaller increases in K282N, an AA change previously linked to escape (Fig. 4b, Bricault et al., 2019). In contrast, locus 279 started with more pre-trial variation and exhibited differing or even opposite responses in different participants. At locus 279, 2C5 and 2E7 experienced increases and decreases, respectively, in 279N frequency following 3BNC117 infusion. Participant 2E3 experienced an increase in 279E, an AA identity not accessible by a single mutation for 2E7, indicating mutational accessibility may shape escape routes.

To further investigate how genetic background impacts which specific AAs confer escape, we compared our identified mutations to those identified via DMS in two different backgrounds (Radford & Bloom, 2025) and found little correspondence (Supp. Fig. 25a). However, at the locus level, loci shared across participants had higher escape scores than single participant loci, although not significantly so (Supp. Fig. 25b). Loci mutated repeatedly across hosts *in vivo* may therefore represent escape routes that confer a fitness benefit across a greater range of genetic backgrounds.

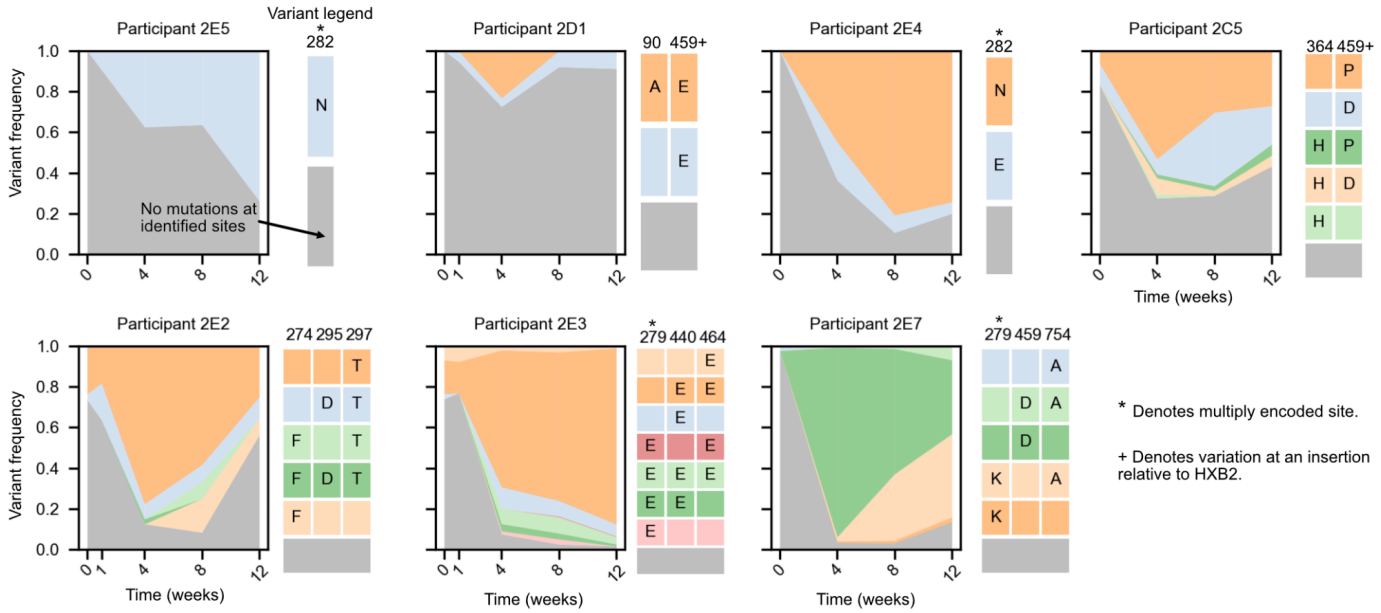

Figure 5. Parallel escape responses are observed in many 3BNC117-treated participants. **Left:** Frequencies of genetic backgrounds carrying positively selected loci identified by MPL or multiple encodings during the trial. Only loci with AAs increasing in frequency by >10% during the trial are shown. **Right:** AA combinations composing the genetic backgrounds plotted at left, matched by color and vertical ordering (mutations away from wild type shown). Starred (*) columns denote AAs with multiple observed nucleotide encodings and pluses ($^{+}$) denote variation at an insertion site relative to HXB2. Sequences within the same variant group can differ at loci not identified by selection scans. Participants 2E1 and 2C1 carried no putative escape mutations exceeding 10% frequency and are not plotted.

Putatively resistant sequences remain at low frequencies in some participants

Despite deeper sequencing, we identified relatively little evidence of genetic response in 2D1 and 2C1. Our selection scans identified no loci in 2C1, and mutations at identified loci in 2D1 never exceeded 25% frequency collectively. Changes in V5 length and glycosylation patterns were inconsistent and minor across these two individuals (Supp. Fig. 22,23). Both 2D1 and 2C1 were previously noted in Caskey et al. 2015 as having slower rebound than other participants, and low IC50s among the small number of isolates individually assayed (Caskey et al., 2015). One potential explanation for the viral load and IC50 dynamics observed during the trial is that, despite therapeutic serum antibody concentrations that would be restrictive *in vitro*, 3BNC117 failed to reach sufficient *in vivo* therapeutic levels in certain participants and may therefore apply only limited selective pressure (Reeves et al., 2023).

Intra-host 3BNC117 escape is often driven by parallel evolutionary responses

Finally, we assessed if evolutionary parallelism underpinned escape in the 3BNC117 cohort by categorizing sequence variants based on which mutations they carried at identified loci under selection. We conservatively excluded the “Additional variation” loci shown in figure 4A due to their relatively weaker evidence for selection and examined only AAs at loci identified by our other scans (MPL or the multiple encoding analysis) that also increased by 10% over the course of the trial. Despite the stringency of our selection scan and inclusion criteria, we nevertheless found evidence of some degree of escape response parallelism in all participants except 2E1 whose only identified loci were “Additional variation” and 2C1 who had minimal genetic response (Fig. 5).

In some instances, this parallelism was driven by multiple AAs at the same locus (2C5 and 2E4), and in other cases it was driven by multiple AAs at different loci that showed some degree of recombination between the identified sites (2E2, 2E7, 2E3). We also observed parallelism in escape responses in participants 2E3, 2E4, 2E5 and 2E7 as evidenced by escape AAs at sites 279 and 282 being encoded by multiple independent nucleotide changes, similar to what was observed in 10-1074. We found similar results when we examined only the subset of loci previously linked to 3BNC117 escape in the literature (except for losing evidence of parallelism in 2E2 and 2D1, Supp. Fig. 26) and when we included the additional linked loci (except for gaining evidence of parallelism in 2E1, Supp. Fig. 27). In 2E2 and 2E5, discovering this parallelism was only possible by virtue of our increased sequencing depth (Supp. Fig. 17, 20). While the degree of escape parallelism shown here is less extreme than the patterns observed in response to 10-1074, HIV populations often do appear to produce and select multiple escape mutations against 3BNC117 simultaneously, albeit at a lower rate.

Discussion

Broadly neutralizing antibodies (bNAbs) are currently in development as both HIV prevention and cure modalities (Julg et al., 2022, 2024; Sneller et al., 2022; Williamson et al., 2025). The emergence of escape mutations in response to single bNAbs parallels early antiretroviral monotherapies, reinforcing the principle that durable suppression of HIV will likely require antibody combinations targeting multiple non-overlapping epitopes. In this study, we used deep haplotype-resolved sequencing to understand viral escape from bNAb monotherapy in people with chronic untreated HIV who received a single infusion of 10-1074 or 3BNC117.

Reanalysis of clinical samples using our long-read SMRT-UMI approach revealed novel HIV evolutionary strategies to evade bNAb pressure. By generating 3.5–7.5 times more sequences than previous methods, we were able to resolve minority variants with clarity and to trace their ontogeny within viral quasispecies. This level of resolution revealed: 1) new evidence of preexisting resistance, 2) previously unrecognized evolutionary parallelism in response to 10-1074, 3) apparent fitness differences between different 10-1074 escape mutations at loci 332 and 334, 4) sites that previously appeared to rapidly dominate the population were actually constrained to much lower frequencies, and 5) new sites that appeared to be under positive selection. Importantly, because our analysis spanned two different bNAbs targeting distinct features of Env, we were able to directly compare how drug-specific selective pressures shape resistance in fundamentally different ways.

For 10-1074, where either the disruption of the GDIR motif at locus 325 or the loss of the N332 glycan are sufficient to confer viral escape, we find these pathways are repeatedly accessed both within and across participants, likely because 10-1074 binding to Env is highly dependent on the highly conserved N332 glycan (Gristick et al., 2016). Strikingly, the number of parallel occurrences of resistance within single viral populations escaping from 10-1074 monotherapy appears considerably higher than HIV responding to early ART therapies, in which parallel emergence of resistance is common (Feder et al., 2016, 2021), but the number of clearly distinguishable origins is often only 1-3 (Pennings et al., 2014; Williams & Pennings, 2020). We further find that comprehensive sampling of accessible 10-1074 escape mutations allows HIV to select those mutations that retain other favorable properties. Mutations that disrupt the GDIR motif and those that remove the N332 glycan have different fitness costs and growth rates (Bricault et al., 2019; Meijers et al., 2021), but our results further suggest that HIV may preferentially select those specific N332 and S334 mutations that preserve cell entry functionality or shift glycans. This finding underscores a major hurdle in developing therapies against HIV: not only is HIV able to escape 10-1074 quickly, but it generates enough mutants to select those that minimize the cost of resistance.

These patterns are not evident in viral responses to 3BNC117, where escape occurs at a much wider array of loci that are often not shared between participants. This suggests that the escape mutations which are available to a viral population may depend on its genetic characteristics at the time of treatment. These findings are consistent with Radford et al.'s DMS, which assayed 3BNC117 against two older HIV backbones from different clades (A and B) and found distinct mutations resulting in escape (deCamp et al., 2014; Li et al., 2005; Sanders et al., 2013; Wu et al., 2006). We similarly found distinct escape mutations in different participants even though all donors in our cohort carried contemporary clade B viruses. However, we observe that similar escape mutations arise within the same individual and in cases where individuals share closely related viral strains, but not in more divergent viruses. For example, we observe a strong response at site 282 exactly shared in a transmission pair (2E5, 2E4), but not found in any other participants. Furthermore, we identify many instances of a single genetic background producing the same escape AA repeatedly via multiple nucleotide encodings while viruses in other participants escape via other mutations. Because genetic context can impact which mutations confer escape, predicting resistance responses from pre-treatment genotyping may therefore be unreliable.

Despite their differences, we found a number of similarities between evolutionary dynamics generating resistance to 3BNC117 and 10-1074 monotherapy. Most notable is the degree of parallelism by which these populations escaped. We observed three forms of evolutionary parallelism resulting in resistance to bNAbs: 1) distinct viruses evolving exactly the same AA mutation at the same locus, both within and across participants, 2) distinct viruses evolving different AA mutations at the same locus; and 3) distinct viruses evolving distinct AA mutations at different loci, but conferring broadly a viral rebound phenotype. Parallelism in response to 10-1074 was more extreme than to 3BNC117, potentially indicating that 10-1074 has a larger target size of accessible and functionally tolerated escape mutations (Hermisson & Pennings, 2017). Alternatively, given our detailed mechanistic understanding of 10-1074 escape, we may simply be better powered to detect escape parallelism in populations treated with 10-1074 than 3BNC117. 3BNC117 escape routes that are highly participant-specific or remain at low overall frequency are challenging to detect given the limitations of our tools.

A second important similarity between viral responses to both 10-1074 and 3BNC117 is that we discovered viral populations that harbored rare pre-existing resistance mutations to both bNAbs at day 0 (3/11 harbored detectable resistance mutations to 10-1074 and 2/9 harbored putative resistance mutations to 3BNC117). This was potentiated by deeper sequencing, but any attempt to sequence a viral population *ex vivo* will be incomplete and comprehensively profiling rare mutations is unrealistic. While this appears to present an obstacle for predicting viral responses to bNAb therapy, surprisingly, we found that rare pre-treatment resistance mutations for 10-1074 did not predict which mutations reached highest frequencies after treatment. In agreement with our parallelism results, this finding suggests that large viral populations can readily produce escape mutations to certain bNAbs and that attempting to screen for rare pre-existing mutations may provide limited additional information.

We note two important caveats for this study. First, we cannot unequivocally establish neutralization or escape beyond previously published neutralization data. For 10-1074, escape mutations at loci 325, 332, and 334 have been well documented in the literature as conferring complete resistance to 10-1074 (Bricault et al., 2019; Caskey et al., 2017; Dingens et al., 2019; Radford & Bloom, 2025; Selzer et al., 2025). For 3BNC117, we cross referenced our findings with existing DMS and neutralization studies, but we can only classify variants as escape-associated, and we cannot strongly assert that any single mutation causes escape from 3BNC117. This is a challenge shared with other *in silico* escape prediction approaches (Bai et al., 2019; Magaret et al., 2019; Moldt et al., 2021). Second, discriminating between neutral and selective dynamics is inherently challenging, even when equipped with comprehensive time series data. Rapid changes in viral population sizes can result in large allele frequency fluctuations even under neutral conditions (Swan et al., 2022). We

account for this by using a strong selection coefficient cut off in evaluating our MPL results. While this conservative approach may result in missing 3BNC117 escape mutations experiencing more subtle changes, lowering this threshold will likely generate false positives by identifying frequency changes that occurred via neutral drift instead of selection. These two challenges are compounded when evaluating viral backbones that carry multiple putative escape mutations rising in frequency together, resulting from synergistic interactions among the mutations, or simply genetic hitchhiking. While we do find new associations for changes that occurred in multiple participants or reached high frequency within participants, we cannot definitively conclude whether these variants specifically drove escape or changed in frequency during the trial for other reasons.

What does this tell us about administering combination antibody therapies? First, deeper sequencing enabled us to show that preexisting resistance mutations are more common than originally thought (Julg et al., 2024; Mendoza et al., 2018; Saha & Dixit, 2020). Second and relatedly, viral populations escaping from both 10-1074 and 3BNC117 can accrue many simultaneous mutations that associate with escape. Similar to observations noted in the development of cART, this degree of parallelism and preexisting resistance underscores the importance of combining multiple challenges to the virus simultaneously. This approach has been promising in combination therapy clinical trials occurring after the two profiled here, although resistance evolution remains an ongoing challenge, supporting the conclusion that including a third challenge, either via the host's humoral immune response or an additional therapy, is necessary for sustained, durable viral remission (Bertagnolli et al., 2020; Eron et al., 2024). Because escape from 10-1074 appears more parallel than escape from early ART, it is possible that the combinatorial challenge necessary for some bNAbs combinations might be even higher. Third, information about the number of mutations conferring escape to a given bNAb and the rate at which those mutations emerge has been incorporated into computational models that predict optimal bNAbs combination therapies (LaMont et al., 2022). If the number of accessible mutations or their rate of emergence is highly variable across viral genetic backgrounds, these models may need to be adjusted to account for participant-specific variation. Last, direct screening for pre-existing resistance genotypically may present substantial challenges to identifying prospective combination therapy recipients who are sensitive to all antibody components.

Several trials have now combined bNAbs targeting two or three non-overlapping epitopes either as primary therapy or after an ART interruption (Bar-On et al., 2018; Gaebler et al., 2022; Julg et al., 2024; Mendoza et al., 2018; Sneller et al., 2022). These combinations can achieve sustained periods of ART-free remission in certain people living with HIV, but some viral populations nevertheless rebound prematurely, especially those treated with two bNAb therapies. While our results highlight the substantial challenges in applying bNAb combination therapies broadly, bNAb-ART combination therapies still hold promise: 10-1074 and 3BNC117 supplemented with the long-acting ART drug lenacapavir (Eron et al., 2024), or VRC07.523LS and cabotegravir (Taiwo et al., 2025), resulted in sustained viral suppression, and showed that antibodies can be combined safely and effectively with small molecule therapies. Dual bNAbs applied with an immune-modulation TLR9 agonist enabled post-intervention control in 7 of 10 therapy recipients (Peluso et al., 2025). Furthermore, bNAbs potentially offer functions beyond viral suppression such as engaging and possibly stimulating the host immune response, and when the virus is highly sensitive they may achieve outcomes that rival or exceed ART (Lu et al., 2016; Niessl et al., 2020; Rosás-Umbert et al., 2022; Schoofs et al., 2016; Tebas, 2025). Therefore, despite the obstacles currently preventing broadscale administration of bNAbs, deep sequencing of resistance profiles to determine how HIV evades these antibodies lays an important foundation for the rational design of next-generation antibody combinations and adjunctive strategies to achieve durable, ART-free remission.

Methods

Sample selection

All participants were provided informed consent and the parental studies (Caskey et al., 2015, 2017) were approved by the Rockefeller University IRB.

MCA-0885
Plasma samples were selected from 12 participants in a phase 1 clinical trial testing a single 10-1074 broadly neutralizing antibody (bNAb) infusion in viremic participants living with HIV-1 (NCT 02511990, Caskey et al., 2017). Baseline and subsequent timepoints were sequenced. (Fig. 1b, Supplemental table 1).

MCA-0835
Plasma samples were selected from 7 participants in a phase 1 clinical trial testing a single 3BNC117 bNAb infusion in viremic participants living with HIV-1 (NCT 02018510, Caskey et al., 2015). Baseline and subsequent timepoints were sequenced (Fig. 1b, Supplemental table 2).

RNA isolation and cDNA synthesis

Frozen plasma samples (1mL) were thawed and viral RNA isolated using MinElute Virus Spin kits (Qiagen, #55704) or Viral RNA Mini spin kits (Qiagen, #52904). cDNA synthesis performed from viral RNA using HIV-1 specific oligos or SMRT-UMI cDNA 5' ultramers comprised an HIV-1 specific binding region, an 8bp random nucleotide UMI, a 6bp sample ID, and two reverse primer binding regions (Westfall et al., 2024). cDNA was synthesized using SuperScript IV Reverse Transcriptase (10U/uL, Thermo Fisher Scientific), supplemented with SUPERaseIn RNAse Inhibitor (1U/uL, Thermo Fisher Scientific), ThermaStop RT (0.2U/uL, Millapore Sigma, discontinued) and standard or SMRT-UMI oligos (0.4uM, IDT). cDNA reactions were incubated for 1 hour at 50C, then inactivated at 80C for 10 minutes. RNA was removed with RNase H for 20 min at 37C (0.1U/uL, Thermo Fisher Scientific) and cDNA purified using RNAClean XP beads (Beckman Coulter) at a 1:1 ratio and washed 3x with 80% ethanol.

Amplification

HIV *env* cDNA concentration was estimated using an end point dilution 25uL nested PCR using PrimeSTAR GXL polymerase (1.25U/uL, Takara Bio Inc), a 1uL cDNA input, and 0.25uM forward and reverse PCR 1 primers as previously described (PMID: 38765465). End point nested PCR was performed at the following cycling conditions for PCR 1: 2min at 98C; 35 cycles of 10 sec at 98C, 15 sec at 60C, and 3:15min at 68C; 7 min at 68C; 4C hold. The following cycling conditions were performed for PCR 2 with a 1uL PCR 1 input and forward and reverse PCR 2 primers: 2min at 98C; 35 cycles of 10 sec at 98C, 15 sec at 62C, and 3:15min at 68C; 7 min at 68C; 4C hold. Positive end point dilution reactions were defined as a 3kb band visualized by gel electrophoresis (Rodrigo et al., 1997) and used to estimate cDNA concentration using the Quality webtool (https://quality.fredhutch.org/).

Samples with low viral load, where cDNA was synthesized without SMRT-UMI oligos, were amplified at limiting dilution, to ensure positive PCRs contained only a single cDNA template, according to the PCR conditions listed above. PCR 2 primers contained 5' tag sequences complementary to unique index primers added during a third PCR to allow for pooling of positive PCRs for sequencing.

For SMRT-UMI sequencing, an estimated 50 HIV *env* cDNA molecules were input into each 25uL PCR reaction and were amplified using 0.25uM forward and reverse PCR 1 primers at the following cycling

conditions: 2min at 98C; 20 cycles of 10 sec at 98C, 15 sec at 60C, and 3:15min at 68C; 7 min at 68C; 4C hold. First-round PCR product was pooled and cleaned by magnetic bead size selection (AMPure XP, 0.5x) and a second-round PCR was performed using 1uL of bead cleaned 1st round product and 0.25uM second round PCR primers at the following cycling conditions: 2min at 98C; 20 cycles of 10 sec at 98C, 15 sec at 62C, and 3:15min at 68C; 7 min at 68C; 4C hold.
A heteroduplex resolution step was conducted at the end of the second PCR, which consisted of spiking in PrimeSTAR GXL, 2nd round forward and reverse primers and dNTPs to each reaction tube and incubating for: 2min at 98C; 15s at 62C; 10min at 68C; and a 4C hold. Final amplified products were confirmed by a 3kb band visualized by gel electrophoresis and purified by magnetic bead size selection (AMPure XP magnetic beads, 0.7x).

All cDNA and PCR primers ordered from IDT and listed in **Supp. Table 10**. Index primers listed along with demultiplexing pipeline at https://github.com/lcohnlab/sga-pipeline.

Method validation

To validate our methods, we performed several quality control experiments. First, to determine whether recombination occurs during reverse transcription, we combined RNA from two infectious molecular clones, 89.6 (Collman et al., 1992) and LAI.2 (Wain-Hobson et al., 1985), for cDNA synthesis, performed single genome amplification (REF) on the resulting cDNA, and sequenced single viral envelope genes by Illumina MiSeq. Compared to the reference 89.6 and LAI.2 genomes, no 89.6/LAI.2 recombinants were identified, demonstrating a negligible amount of recombination during cDNA synthesis (Supp. Fig. 28a).

We then tested the ability of our adapted PORPIDpipeline to filter out PCR recombinants during bulk amplification (Westfall et al., 2024, adaptations in methods). To test the filtering capacity of the pipeline, we combined 89.6 and LAI.2 cDNA which contained different sample ID barcodes and processed them with bulk PCR amplification. These were sequenced by PacBio and subsequently analyzed. Compared with the reference 89.6 and LAI.2 envelope sequences, we observed no recombinant sequences identified following PORPID filtering (Supp. Fig. 28b).

Sample pooling

PCR product was quantified using the Qubit HS 1x dsDNA assay (ThermoFisher). Up to 16 SMRT-UMI sample IDs or 384 individually indexed PCR were pooled in equimolar amounts in a ratio equivalent to the estimated number of templates input into that sample's PCR. Only one timepoint from each participant was included in each pool to avoid incorrect identification of samples as contamination by bioinformatic processing.

Library prep

Libraries were prepared using the SMRTBell Express Template Prep kit 2.0 (Pacific Biosciences). Sample pools were divided into 90ng input reactions (10uL each) and barcoded using the Barcoded Overhang Adaptor Kit - 8A (Pacific Biosciences). Libraries were sequenced using a PacBio Sequel IIe (Fred Hutchinson Cancer Center Genomics and Bioinformatics Core Facility).

Sequence generation and sequence preparation

Demultiplexing and consensus generation was performed from PacBio CCS reads separately from single positive PCR or samples amplified in bulk with SMRT-UMI oligos. Reads from single positive PCRs used a simple pipeline (https://github.com/lcohnlab/sga-pipeline), while the PORPIDpipeline software was adapted to run on a local cluster for samples amplified in bulk. PORPIDpipeline performs read quality filtering, read demultiplexing by sample and UMI, exclusion of erroneous UMI, consensus sequence generation for each

UMI, contamination check, sequence quality filtering, and report generation as previously described (Westfall et al., 2024). Additional sequence filtering took place for each SMRT-UMI sample using custom R scripts. First, the sequences were ordered from those with the most reads contributing to their consensus to those with the least. Next, the sequences consisting of the bottom 15% or 25% of total reads were excluded, depending on which cutoff excluded the lowest tail of the read distribution best. Adapted PORPIDpipeline software and additional filtering scripts available at https://github.com/lcohnlab/PORPIDPipeline_Cluster-AC-2025.

High-quality consensus sequences from PORPID for each participant were trimmed to matching autologous *env* sequences (Caskey et al., 2015, 2017; Schoofs et al., 2016) and aligned to HXB2 reference genome *env* sequence using MUSCLE 5.1 (AliView Alignment Viewer, Larsson, 2014). Sequences with premature stop codons or frameshift mutations following polynucleotide sequences of 4 or more identical nucleotides were frameshift corrected. Nucleotide sequences were translated to corresponding amino acid sequences and re-aligned to the HXB2 reference *env* amino acid sequence. We excluded sequences with internal deletions totaling more than 3% of the *env* sequence as well as insertions greater than 3% of the sequence.

Sequencing validation

A variety of validations of the SMRT-UMI protocol were performed to confirm the efficacy of the Probabilistic Offspring Resolver for Primer IDs (PORPID pipeline) of sorting out recombinant sequences. We confirmed that there was a negligible amount of recombination during cDNA synthesis, and any in vitro recombinants formed during PCR were sorted out by PORPID (Supp. Fig. 28a,b). Validated sequences were compared to sequences originally recovered using single genome amplification (SGA) to determine if the two sequencing approaches recovered similar viral populations at the same time point using a pairwise panmixia test (Caskey et al., 2015, 2017; Kearney et al., 2014; Schoofs et al., 2016, FDR-adjusted $p < 1 \times 10^{-4}$). Of the samples with matched SGA sequences, 34/43 were found to have no significant compartmentalization between sequencing methods. Of those that were significantly compartmentalized, the inadequate sample size of SGA or the presence of a subclade found by SMRT-UMI not found with SGA contributed to the compartmentalization (Supp. Fig. 2).

Code availability

All additional code for conducting analyses listed below is available at https://github.com/evromero-uw/hiv_bnabs_paper_archive.git.

Sequence alignment and phylogenetic analysis

Within host *env* nucleotide sequences were codon-aligned using MUSCLE v5 and then manually inspected and edited using AliView. SMRT-UMI sequences, recovered here, were aligned along with available full *env* SGA sequences from NCT 02511990 participants collected in Caskey et al., 2017 and from NCT 02018510 participants collected in Schoofs et al., 2016 & Caskey et al., 2015. Phylogenetic trees were created using IqTree2 (Minh et al., 2020) and plotted using the R packages ape and phytools (Paradis & Schliep, 2019; Revell, 2024). All HXB2 positions reported are relative to the start of the *env* gene and gaps with respect to HXB2 are reported as outlined by the LANL HIV database (*Numbering Positions in HIV Relative to HXB2CG*, n.d.).

Identification of potential escape loci

We analyzed sequence alignment positions with <10% gaps that contained a majority allele at frequency ≥50% at day 0, indicating good alignment quality. For each position in each participant, we determined the majority AA at day 0 and then calculated the proportion of sites differing from majority AA at any subsequent timepoint. We report sites experiencing a majority AA loss of >0.4 in the 10-1074 cohort and >0.05 in the 3BNC117

cohort. Despite using a highly inclusive threshold for the 3BNC117 cohort, this analysis yielded no sites that were variable in the majority of participants, prompting an additional selection scan.

For the 3BNC117 cohort, we ran an additional selection scan using MPL with run parameters matching those used by Sohail et al., 2021 (mutation rates from Zanini et al., 2017, $N_e = 1 \times 10^4$, gaussian regularization strength $g = 5 \times 10^4$, <95% alignment column gap frequency, >3 sequences/time point). We examined sequencing data up to week 8 to capture only those dates with therapeutic bNAb serum concentrations. Sequences for participant 2D1 were truncated at HXB2 nucleotide position 1530 prior to MPL analysis since trial day 0 sequencing data was not available past this locus. We chose a filtering cutoff of $s \geq 0.044$ to identify sites where positive selection would be strong enough to create a substantial frequency increase during the trial (reaching or exceeding 15% frequency from 5% over 8 weeks or 28 generations under a drift-free, discrete generation model of haploid reproduction, Felsenstein, 2019, p.58). We also ran a single locus variant of MPL where linkage between sites is ignored (the off-diagonal entries of the covariance matrix are set to 0, but all other parameters remain the same). We report sites in 3BNC117 contact regions which passed our $s \geq 0.044$ threshold in the single locus analysis, but not the full MPL analysis, denoting them as “additional variation”. These additional sites are excluded from downstream analyses unless specifically noted.

We determined a site as having literature support for escaping a given bNAb if it either 1) had a significant escape score, as determined by dms_tools2 findSigSel, against the relevant bNAb in a recent DMS experiment (Bloom, 2015; Radford & Bloom, 2025), or was reported as escape-associated in 2) the LANL HIV antibody contact database (Bricault et al., 2019; Dingens et al., 2019; LaBranche et al., 2018; Los Alamos National Laboratory, n.d.; Schommers et al., 2020) or the LANL CATNAP IC50 data by the antibody database program (West et al., 2013; Yoon et al., 2015, run parameters: min residue freq = 1%, max # of rules= 10, free set = 20%). We denote sites identified by the above methods that also had literature support as “putative escape loci”.

Variable loop characterization

Potential N-linked glycosylation sites (PNGs) were identified via the canonical NX[ST] amino acid motif, where X is any amino acid excluding proline (Bause & Hettkamp, 1979). Any participant where the majority PNG pattern at day 0 changed in frequency by 10% or more during the trial was denoted as having shifts in glycosylation patterns.

Analysis of 10-1074 mutational probabilities

We computed the relative probabilities of mutating away from N332 or S334 via all possible single step nucleotide substitutions based on participant-specific codons present at day 0 and HIV-specific mutation rate estimates (Zanini et al., 2017). Codons for escape mutations present at day 0 were excluded from the analysis. Expected relative frequencies of escape AAs at sites 332 and 334 in each participant were then calculated by weighting the mutation rate-adjusted accessible escape AAs for each ancestral codon by its participant-specific day 0 frequency. Enrichment as plotted in figure 2 was calculated as the log ratio of observed to expected AA frequency in each participant. To test the statistical support for enrichment, we tested if the proportion of escape sequences at a given site with a specific AA identity was higher than its expectation using a one-sided binomial test with Bonferroni correction, after pooling the observed counts and taking a sample size weighted average of the expected proportions across participants.

Multiply encoded variant analysis

We identified all AA identities within a participant sampled only after day 0 and determined if multiple distinct nucleotide changes from codon triplets present at day 0 could produce the AA substitution. We restricted this analysis to newly appearing AAs to minimize the impact of secondary synonymous substitutions. Sites were reported as multiply-encoded if at least two sequences carried two or more different nucleotide encodings, and singly encoded otherwise. Sites in poorly aligned regions were excluded.

Ancestor network analysis

We traced haplotypes carrying 10-1074 escape mutations in a 300bp window flanking the GDIR motif and 332 glycan (HXB2 nucleotide coordinates 825-1152 with sites 975-1002 masked). This window size was chosen to minimize the impact of viral recombination during the initial four weeks of therapeutic response given existing estimates of HIV generation time and recombination rate (Perelson et al., 1996; Romero & Feder, 2024), but our results were qualitatively robust to window size. Each sequence sampled at weeks 1 and 4 was assigned to its closest ancestor at any previous time point via minimum hamming distance. Sequences equidistant from multiple ancestors were assigned to all possible ancestors. The haplotype network graph was formed with each node representing a unique 300 bp motif and each edge connecting a descendant motif to its closest matched ancestor. Each connected component of the network represents a single lineage deriving from day 0 and consists of sequence motifs more closely related to each other than to any others sampled.

We tested if 10-1074 escape alleles appeared on more day 0 sequence motifs than non-escape alleles, controlling for allele frequency. We repeated the network analysis described above in which we centered 300bp windows on all sites of non-escape variation and determined the number of day 0 lineages on which non-escape alleles appeared. We compared escape and non-escape alleles by fitting the following linear regression:

$$\#\ Day\ 0\ lineages \sim \beta_0 + \beta_1 \cdot f + \beta_2 \cdot f \cdot I_{escape} + \varepsilon$$

in which f represents the maximum frequency of an allele at any point during the trial, and I_{escape} is an indicator variable of whether or not the allele is associated with escape. We report the strength, directionality and significance of the interaction coefficient, β_2.

3BNC117 haplotype analysis

We report haplotypes composed of all alleles at putative escape loci which were not the majority alleles at day 0 and increased in frequency by at least 10% (with support from at least two sequencing reads at the given timepoint) during the trial.

Comparison to deep mutational scanning data

Published DMS data for TRO11 and BF520 HIV Env proteins was filtered based on author recommendations to include only AA variants observed at least 2 times in the TRO11 dataset and 3 times in the BF520 dataset (Radford & Bloom, 2025). For AA level analyses, mean escape scores across DMS replicates were compared to frequency changes of matched AAs at the same HXB2 coordinates in the in vivo trials. For locus level analyses, the maximum escape score (maximum of all mean escape scores for AAs at the given locus across both envelope strains) was used.

Acknowledgements

We thank all of the study participants who participated in the first-in-human trials of 10-1074 and 3BNC117; the Rockefeller University Hospital nursing staff and Clinical Research Support Office and nursing staff; Deysi Dubon for laboratory support, Anthony West, Daniel Reeves, John P. Barton, Pleuni S. Pennings, and Michel Nussenzweig for critical reading of our manuscript; all members of the Feder and Cohn labs, Alexis Chang, Caelan Radford, and Jesse Bloom for helpful discussion; Wenjie Deng for bioinformatics support. This work was supported in part by the following NIH NIAID grants UM1AI64565 and U01AI169385 to LBC and MC, the Pew Research Scholars Program to LBC, and NIH 1DP2CA280623-01 and the Gilead Sciences Research Scholars Program in HIV to AFF; This work was additionally supported by the Genomics and Bioinformatics Shared Resource (Research Resource Identifier [RRID]:SCR_022606) of the Fred Hutchinson Cancer Center/University of Washington/Seattle Children's Cancer Consortium funded by the National Cancer Institute (grant number P30 CA01570).

References

Bai, H., Lewitus, E., Li, Y., Thomas, P. V., Zemil, M., Merbah, M., Peterson, C. E., Thuraisamy, T., Rees, P. A., Hajduczki, A., Dussupt, V., Slike, B., Mendez-Rivera, L., Schmid, A., Kavusak, E., Rao, M., Smith, G., Frey, J., Sims, A., … Rolland, M. (2024). Contemporary HIV-1 consensus Env with AI-assisted redesigned hypervariable loops promote antibody binding. *Nature Communications*, *15*(1), 3924. https://doi.org/10.1038/s41467-024-48139-x

Bai, H., Li, Y., Michael, N. L., Robb, M. L., & Rolland, M. (2019). The breadth of HIV-1 neutralizing antibodies depends on the conservation of key sites in their epitopes. *PLOS Computational Biology*, *15*(6), e1007056. https://doi.org/10.1371/journal.pcbi.1007056

Bar-On, Y., Gruell, H., Schoofs, T., Pai, J. A., Nogueira, L., Butler, A. L., Millard, K., Lehmann, C., Suárez, I., Oliveira, T. Y., Karagounis, T., Cohen, Y. Z., Wyen, C., Scholten, S., Handl, L., Belblidia, S., Dizon, J. P., Vehreschild, J. J., Witmer-Pack, M., … Nussenzweig, M. C. (2018). Safety and antiviral activity of combination HIV-1 broadly neutralizing antibodies in viremic individuals. *Nature Medicine*, *24*(11), 1701–1707. https://doi.org/10.1038/s41591-018-0186-4

Bause, E., & Hettkamp, H. (1979). Primary structural requirements for N-glycosylation of peptides in rat liver. *FEBS Letters*, *108*(2), 341–344. https://doi.org/10.1016/0014-5793(79)80559-1

Bertagnolli, L. N., Varriale, J., Sweet, S., Brockhurst, J., Simonetti, F. R., White, J., Beg, S., Lynn, K., Mounzer, K., Frank, I., Tebas, P., Bar, K. J., Montaner, L. J., Siliciano, R. F., & Siliciano, J. D. (2020). Autologous IgG antibodies block outgrowth of a substantial but variable fraction of viruses in the latent reservoir for

HIV-1. *Proceedings of the National Academy of Sciences*, *117*(50), 32066–32077. https://doi.org/10.1073/pnas.2020617117

Bloom, J. D. (2015). Software for the analysis and visualization of deep mutational scanning data. *BMC Bioinformatics*, *16*(1), 168. https://doi.org/10.1186/s12859-015-0590-4

Bournazos, S., Wang, T. T., Dahan, R., Maamary, J., & Ravetch, J. V. (2017). Signaling by Antibodies: Recent Progress. *Annual Review of Immunology*, *35*(1), 285–311. https://doi.org/10.1146/annurev-immunol-051116-052433

Bricault, C. A., Yusim, K., Seaman, M. S., Yoon, H., Theiler, J., Giorgi, E. E., Wagh, K., Theiler, M., Hraber, P., Macke, J. P., Kreider, E. F., Learn, G. H., Hahn, B. H., Scheid, J. F., Kovacs, J. M., Shields, J. L., Lavine, C. L., Ghantous, F., Rist, M., … Korber, B. (2019). HIV-1 Neutralizing Antibody Signatures and Application to Epitope-Targeted Vaccine Design. *Cell Host & Microbe*, *25*(1), 59-72.e8. https://doi.org/10.1016/j.chom.2018.12.001

Caskey, M., Klein, F., Lorenzi, J. C. C., Seaman, M. S., West, A. P., Buckley, N., Kremer, G., Nogueira, L., Braunschweig, M., Scheid, J. F., Horwitz, J. A., Shimeliovich, I., Ben-Avraham, S., Witmer-Pack, M., Platten, M., Lehmann, C., Burke, L. A., Hawthorne, T., Gorelick, R. J., … Nussenzweig, M. C. (2015). Viraemia suppressed in HIV-1-infected humans by broadly neutralizing antibody 3BNC117. *Nature*, *522*(7557), 487–491. https://doi.org/10.1038/nature14411

Caskey, M., Schoofs, T., Gruell, H., Settler, A., Karagounis, T., Kreider, E. F., Murrell, B., Pfeifer, N., Nogueira, L., Oliveira, T. Y., Learn, G. H., Cohen, Y. Z., Lehmann, C., Gillor, D., Shimeliovich, I., Unson-O'Brien, C., Weiland, D., Robles, A., Kümmerle, T., … Klein, F. (2017). Antibody 10-1074 suppresses viremia in HIV-1-infected individuals. *Nature Medicine*, *23*(2), 185–191. https://doi.org/10.1038/nm.4268

Chen, X., Zhou, T., Schmidt, S. D., Duan, H., Cheng, C., Chuang, G.-Y., Gu, Y., Louder, M. K., Lin, B. C., Shen, C.-H., Sheng, Z., Zheng, M. X., Doria-Rose, N. A., Joyce, M. G., Shapiro, L., Tian, M., Alt, F. W., Kwong, P. D., & Mascola, J. R. (2021). Vaccination induces maturation in a mouse model of diverse unmutated VRC01-class precursors to HIV-neutralizing antibodies with >50% breadth. *Immunity*, *54*(2), 324-339.e8. https://doi.org/10.1016/j.immuni.2020.12.014

Chun, T.-W., Carruth, L., Finzi, D., Shen, X., DiGiuseppe, J. A., Taylor, H., Hermankova, M., Chadwick, K., Margolick, J., Quinn, T. C., Kuo, Y.-H., Brookmeyer, R., Zeiger, M. A., Barditch-Crovo, P., & Siliciano, R.

F. (1997). Quantification of latent tissue reservoirs and total body viral load in HIV-1 infection. *Nature*, *387*(6629), 183–188. https://doi.org/10.1038/387183a0

Cohn, L. B., Chomont, N., & Deeks, S. G. (2020). The Biology of the HIV-1 Latent Reservoir and Implications for Cure Strategies. *Cell Host & Microbe*, *27*(4), 519–530. https://doi.org/10.1016/j.chom.2020.03.014

Collman, R., Balliet, J. W., Gregory, S. A., Friedman, H., Kolson, D. L., Nathanson, N., & Srinivasan, A. (1992). An infectious molecular clone of an unusual macrophage-tropic and highly cytopathic strain of human immunodeficiency virus type 1. *Journal of Virology*, *66*(12), 7517–7521. https://doi.org/10.1128/jvi.66.12.7517-7521.1992

De Wolf, F., Hogervorst, E., Goudsmit, J., Fenyö, E.-M., Rübsamen-Waigmann, H., HOLMES, H., GALVAO-CASTRO, B., KARITA, E., WASI, C., SEMPALA, S. D. K., BAAN, E., ZORGDRAGER, F., LUKASHOV, V., OSMANOV, S., KUIKEN, C., CORNELISSEN, M., & WHO NETWORK FOR HIV ISOLATION AND CHARACTERIZATION. (1994). Syncytium-Inducing and Non-Syncytium-Inducing Capacity of Human Immunodeficiency Virus Type 1 Subtypes Other Than B: Phenotypic and Genotypic Characteristics. *AIDS Research and Human Retroviruses*, *10*(11), 1387–1400. https://doi.org/10.1089/aid.1994.10.1387

deCamp, A., Hraber, P., Bailer, R. T., Seaman, M. S., Ochsenbauer, C., Kappes, J., Gottardo, R., Edlefsen, P., Self, S., Tang, H., Greene, K., Gao, H., Daniell, X., Sarzotti-Kelsoe, M., Gorny, M. K., Zolla-Pazner, S., LaBranche, C. C., Mascola, J. R., Korber, B. T., & Montefiori, D. C. (2014). Global Panel of HIV-1 Env Reference Strains for Standardized Assessments of Vaccine-Elicited Neutralizing Antibodies. *Journal of Virology*, *88*(5), 2489–2507. https://doi.org/10.1128/jvi.02853-13

Dingens, A. S., Arenz, D., Weight, H., Overbaugh, J., & Bloom, J. D. (2019). An Antigenic Atlas of HIV-1 Escape from Broadly Neutralizing Antibodies Distinguishes Functional and Structural Epitopes. *Immunity*, *50*(2), 520-532.e3. https://doi.org/10.1016/j.immuni.2018.12.017

Eron, J. J., Little, S. J., Crofoot, G., Cook, P., Ruane, P. J., Jayaweera, D., VanderVeen, L. A., DeJesus, E., Zheng, Y., Mills, A., Huang, H., Waldman, S. E., Ramgopal, M., Gorgos, L., Collins, S. E., Baeten, J. M., & Caskey, M. (2024). Safety of teropavimab and zinlirvimab with lenacapavir once every 6 months for HIV treatment: A phase 1b, randomised, proof-of-concept study. *The Lancet HIV*, *11*(3), e146–e155. https://doi.org/10.1016/S2352-3018(23)00293-X

Feder, A. F., Pennings, P. S., & Petrov, D. A. (2021). The clarifying role of time series data in the population genetics of HIV. *PLOS Genetics*, *17*(1), e1009050. https://doi.org/10.1371/journal.pgen.1009050

Feder, A. F., Rhee, S.-Y., Holmes, S. P., Shafer, R. W., Petrov, D. A., & Pennings, P. S. (2016). More effective drugs lead to harder selective sweeps in the evolution of drug resistance in HIV-1. *eLife*, *5*, e10670. https://doi.org/10.7554/eLife.10670

Felsenstein, J. (2019). *Theoretical Evolutionary Genetics*. University of Washington. https://books.google.com/books?id=sqBnzwEACAAJ

Gaebler, C., Nogueira, L., Stoffel, E., Oliveira, T. Y., Breton, G., Millard, K. G., Turroja, M., Butler, A., Ramos, V., Seaman, M. S., Reeves, J. D., Petroupoulos, C. J., Shimeliovich, I., Gazumyan, A., Jiang, C. S., Jilg, N., Scheid, J. F., Gandhi, R., Walker, B. D., … Nussenzweig, M. C. (2022). Prolonged viral suppression with anti-HIV-1 antibody therapy. *Nature*, *606*(7913), 368–374. https://doi.org/10.1038/s41586-022-04597-1

Gristick, H. B., von Boehmer, L., West Jr, A. P., Schamber, M., Gazumyan, A., Golijanin, J., Seaman, M. S., Fätkenheuer, G., Klein, F., Nussenzweig, M. C., & Bjorkman, P. J. (2016). Natively glycosylated HIV-1 Env structure reveals new mode for antibody recognition of the CD4-binding site. *Nature Structural & Molecular Biology*, *23*(10), 906–915. https://doi.org/10.1038/nsmb.3291

Haddox, H. K., Dingens, A. S., Hilton, S. K., Overbaugh, J., & Bloom, J. D. (2018). Mapping mutational effects along the evolutionary landscape of HIV envelope. *eLife*, *7*, e34420. https://doi.org/10.7554/eLife.34420

Hermisson, J., & Pennings, P. S. (2017). Soft sweeps and beyond: Understanding the patterns and probabilities of selection footprints under rapid adaptation. *Methods in Ecology and Evolution*, *8*(6), 700–716. https://doi.org/10.1111/2041-210X.12808

Huang, J., Kang, B. H., Ishida, E., Zhou, T., Griesman, T., Sheng, Z., Wu, F., Doria-Rose, N. A., Zhang, B., McKee, K., O'Dell, S., Chuang, G.-Y., Druz, A., Georgiev, I. S., Schramm, C. A., Zheng, A., Joyce, M. G., Asokan, M., Ransier, A., … Connors, M. (2016). Identification of a CD4-Binding-Site Antibody to HIV that Evolved Near-Pan Neutralization Breadth. *Immunity*, *45*(5), 1108–1121. https://doi.org/10.1016/j.immuni.2016.10.027

Julg, B., Stephenson, K. E., Wagh, K., Tan, S. C., Zash, R., Walsh, S., Ansel, J., Kanjilal, D., Nkolola, J., Walker-Sperling, V. E. K., Ophel, J., Yanosick, K., Borducchi, E. N., Maxfield, L., Abbink, P., Peter, L.,

Yates, N. L., Wesley, M. S., Hassell, T., … Barouch, D. H. (2022). Safety and antiviral activity of triple combination broadly neutralizing monoclonal antibody therapy against HIV-1: A phase 1 clinical trial. *Nature Medicine*, *28*(6), 1288–1296. https://doi.org/10.1038/s41591-022-01815-1

Julg, B., Walker-Sperling, V. E. K., Wagh, K., Aid, M., Stephenson, K. E., Zash, R., Liu, J., Nkolola, J. P., Hoyt, A., Castro, M., Serebryannyy, L., Yanosick, K., Speidel, T., Borducchi, E. N., Murzda, T., Maxfield, L., Arduino, R., McDermott, A. B., Gama, L., … Barouch, D. H. (2024). Safety and antiviral effect of a triple combination of HIV-1 broadly neutralizing antibodies: A phase 1/2a trial. *Nature Medicine*, *30*(12), 3534–3543. https://doi.org/10.1038/s41591-024-03247-5

Kearney, M. F., Spindler, J., Shao, W., Yu, S., Anderson, E. M., O'Shea, A., Rehm, C., Poethke, C., Kovacs, N., Mellors, J. W., Coffin, J. M., & Maldarelli, F. (2014). Lack of Detectable HIV-1 Molecular Evolution during Suppressive Antiretroviral Therapy. *PLOS Pathogens*, *10*(3), e1004010. https://doi.org/10.1371/journal.ppat.1004010

Laakso, M. M., Lee, F.-H., Haggarty, B., Agrawal, C., Nolan, K. M., Biscone, M., Romano, J., Jordan, A. P. O., Leslie, G. J., Meissner, E. G., Su, L., Hoxie, J. A., & Doms, R. W. (2007). V3 Loop Truncations in HIV-1 Envelope Impart Resistance to Coreceptor Inhibitors and Enhanced Sensitivity to Neutralizing Antibodies. *PLOS Pathogens*, *3*(8), e117. https://doi.org/10.1371/journal.ppat.0030117

LaBranche, C. C., McGuire, A. T., Gray, M. D., Behrens, S., Zhou, T., Sattentau, Q. J., Peacock, J., Eaton, A., Greene, K., Gao, H., Tang, H., Perez, L. G., Saunders, K. O., Mascola, J. R., Haynes, B. F., Stamatatos, L., & Montefiori, D. C. (2018). HIV-1 envelope glycan modifications that permit neutralization by germline-reverted VRC01-class broadly neutralizing antibodies. *PLOS Pathogens*, *14*(11), e1007431. https://doi.org/10.1371/journal.ppat.1007431

LaMont, C., Otwinowski, J., Vanshylla, K., Gruell, H., Klein, F., & Nourmohammad, A. (2022). Design of an optimal combination therapy with broadly neutralizing antibodies to suppress HIV-1. *eLife*, *11*, e76004. https://doi.org/10.7554/eLife.76004

Larsson, A. (2014). AliView: A fast and lightweight alignment viewer and editor for large datasets. *Bioinformatics*, *30*(22), 3276–3278. https://doi.org/10.1093/bioinformatics/btu531

Li, M., Gao, F., Mascola, J. R., Stamatatos, L., Polonis, V. R., Koutsoukos, M., Voss, G., Goepfert, P., Gilbert, P., Greene, K. M., Bilska, M., Kothe, D. L., Salazar-Gonzalez, J. F., Wei, X., Decker, J. M., Hahn, B. H.,

& Montefiori, D. C. (2005). Human Immunodeficiency Virus Type 1 env Clones from Acute and Early Subtype B Infections for Standardized Assessments of Vaccine-Elicited Neutralizing Antibodies. *Journal of Virology*, *79*(16), 10108–10125. https://doi.org/10.1128/jvi.79.16.10108-10125.2005

Los Alamos National Laboratory. (n.d.). *HIV Molecular Immunology Database*. Retrieved August 13, 2025, from https://www.hiv.lanl.gov/content/immunology/

Lu, C.-L., Murakowski, D. K., Bournazos, S., Schoofs, T., Sarkar, D., Halper-Stromberg, A., Horwitz, J. A., Nogueira, L., Golijanin, J., Gazumyan, A., Ravetch, J. V., Caskey, M., Chakraborty, A. K., & Nussenzweig, M. C. (2016). Enhanced clearance of HIV-1–infected cells by broadly neutralizing antibodies against HIV-1 in vivo. *Science*, *352*(6288), 1001–1004. https://doi.org/10.1126/science.aaf1279

Lynch, R. M., Boritz, E., Coates, E. E., DeZure, A., Madden, P., Costner, P., Enama, M. E., Plummer, S., Holman, L., Hendel, C. S., Gordon, I., Casazza, J., Conan-Cibotti, M., Migueles, S. A., Tressler, R., Bailer, R. T., McDermott, A., Narpala, S., O'Dell, S., … VRC 601 STUDY TEAM. (2015). Virologic effects of broadly neutralizing antibody VRC01 administration during chronic HIV-1 infection. *Science Translational Medicine*, *7*(319), 319ra206-319ra206. https://doi.org/10.1126/scitranslmed.aad5752

Magaret, C. A., Benkeser, D. C., Williamson, B. D., Borate, B. R., Carpp, L. N., Georgiev, I. S., Setliff, I., Dingens, A. S., Simon, N., Carone, M., Simpkins, C., Montefiori, D., Alter, G., Yu, W.-H., Juraska, M., Edlefsen, P. T., Karuna, S., Mgodi, N. M., Edugupanti, S., & Gilbert, P. B. (2019). Prediction of VRC01 neutralization sensitivity by HIV-1 gp160 sequence features. *PLOS Computational Biology*, *15*(4), e1006952. https://doi.org/10.1371/journal.pcbi.1006952

Mahomed, S., Garrett, N., Capparelli, E. V., Osman, F., Harkoo, I., Yende-Zuma, N., Gengiah, T. N., Archary, D., Samsunder, N., Baxter, C., Mkhize, N. N., Modise, T., Carlton, K., McDermott, A., Moore, P. L., Karim, Q. A., Barouch, D. H., Fast, P. E., Mascola, J. R., … Abdool Karim, S. S. (2022). Safety and Pharmacokinetics of Monoclonal Antibodies VRC07-523LS and PGT121 Administered Subcutaneously for Human Immunodeficiency Virus Prevention. *The Journal of Infectious Diseases*, *226*(3), 510–520. https://doi.org/10.1093/infdis/jiac041

Mayer, B. T., deCamp, A. C., Huang, Y., Schiffer, J. T., Gottardo, R., Gilbert, P. B., & Reeves, D. B. (2022). Optimizing clinical dosing of combination broadly neutralizing antibodies for HIV prevention. *PLOS*

Computational Biology, *18*(4), e1010003. https://doi.org/10.1371/journal.pcbi.1010003

Meijers, M., Vanshylla, K., Gruell, H., Klein, F., & Lässig, M. (2021). Predicting in vivo escape dynamics of HIV-1 from a broadly neutralizing antibody. *Proceedings of the National Academy of Sciences*, *118*(30), e2104651118. https://doi.org/10.1073/pnas.2104651118

Mendoza, P., Gruell, H., Nogueira, L., Pai, J. A., Butler, A. L., Millard, K., Lehmann, C., Suárez, I., Oliveira, T. Y., Lorenzi, J. C. C., Cohen, Y. Z., Wyen, C., Kümmerle, T., Karagounis, T., Lu, C.-L., Handl, L., Unson-O'Brien, C., Patel, R., Ruping, C., … Nussenzweig, M. C. (2018). Combination therapy with anti-HIV-1 antibodies maintains viral suppression. *Nature*, *561*(7724), 479–484. https://doi.org/10.1038/s41586-018-0531-2

Minh, B. Q., Schmidt, H. A., Chernomor, O., Schrempf, D., Woodhams, M. D., von Haeseler, A., & Lanfear, R. (2020). IQ-TREE 2: New Models and Efficient Methods for Phylogenetic Inference in the Genomic Era. *Molecular Biology and Evolution*, *37*(5), 1530–1534. https://doi.org/10.1093/molbev/msaa015

Moldt, B., Parvangada, A., Martin, R., Pace, C., Balakrishnan, M., Thomsen, N. D., E. Collins, S., Kuster, H., Braun, D. L., Günthard, H. F., Geleziunas, R., & Callebaut, C. (2021). Evaluation of Broadly Neutralizing Antibody Sensitivity by Genotyping and Phenotyping for Qualifying Participants to HIV Clinical Trials. *JAIDS Journal of Acquired Immune Deficiency Syndromes*, *88*(1), 61. https://doi.org/10.1097/QAI.0000000000002722

Niessl, J., Baxter, A. E., Mendoza, P., Jankovic, M., Cohen, Y. Z., Butler, A. L., Lu, C.-L., Dubé, M., Shimeliovich, I., Gruell, H., Klein, F., Caskey, M., Nussenzweig, M. C., & Kaufmann, D. E. (2020). Combination anti-HIV-1 antibody therapy is associated with increased virus-specific T cell immunity. *Nature Medicine*, *26*(2), 222–227. https://doi.org/10.1038/s41591-019-0747-1

Numbering Positions in HIV Relative to HXB2CG. (n.d.). Retrieved August 13, 2025, from https://www.hiv.lanl.gov/content/sequence/HIV/REVIEWS/HXB2.html

Paradis, E., & Schliep, K. (2019). ape 5.0: An environment for modern phylogenetics and evolutionary analyses in R. *Bioinformatics*, *35*(3), 526–528. https://doi.org/10.1093/bioinformatics/bty633

Parallel Evolution—An overview | ScienceDirect Topics. (n.d.). Retrieved August 13, 2025, from https://www.sciencedirect.com/topics/agricultural-and-biological-sciences/parallel-evolution

Peluso, M., Sandel, D., Deitchman, A., Kim, S. J., Dalhuisen, T., Tummala, H., Tiburcio, R., Zemelko, L., Borgo,

G., Singh, S., Schwartz, K., Deswal, M., Williams, M., Hoh, R., Shimoda, M., Narpala, S., Serebryannyy, L., Khalili, M., Vendrame, E., … Rutishauser, R. (2025). *Combination immunotherapy induces post-intervention control of HIV*. Research Square. https://doi.org/10.21203/rs.3.rs-6141479/v1

Pennings, P. S., Kryazhimskiy, S., & Wakeley, J. (2014). Loss and Recovery of Genetic Diversity in Adapting Populations of HIV. *PLOS Genetics*, *10*(1), e1004000. https://doi.org/10.1371/journal.pgen.1004000

Perelson, A. S., Neumann, A. U., Markowitz, M., Leonard, J. M., & Ho, D. D. (1996). HIV-1 Dynamics in Vivo: Virion Clearance Rate, Infected Cell Life-Span, and Viral Generation Time. *Science*, *271*(5255), 1582–1586.

Radford, C. E., & Bloom, J. D. (2025). Comprehensive maps of escape mutations from antibodies 10-1074 and 3BNC117 for Envs from two divergent HIV strains. *Journal of Virology*, *99*(5), e00195-25. https://doi.org/10.1128/jvi.00195-25

Reeves, D. B., Mayer, B. T., deCamp, A. C., Huang, Y., Zhang, B., Carpp, L. N., Magaret, C. A., Juraska, M., Gilbert, P. B., Montefiori, D. C., Bar, K. J., Cardozo-Ojeda, E. F., Schiffer, J. T., Rossenkhan, R., Edlefsen, P., Morris, L., Mkhize, N. N., Williamson, C., Mullins, J. I., … Edupuganti, S. (2023). High monoclonal neutralization titers reduced breakthrough HIV-1 viral loads in the Antibody Mediated Prevention trials. *Nature Communications*, *14*(1), 8299. https://doi.org/10.1038/s41467-023-43384-y

Revell, L. J. (2024). phytools 2.0: An updated R ecosystem for phylogenetic comparative methods (and other things). *PeerJ*, *12*, e16505. https://doi.org/10.7717/peerj.16505

Rodrigo, A. G., Goracke, P. C., Rowhanian, K., & Mullins, J. I. (1997). Quantitation of target molecules from polymerase chain reaction-based limiting dilution assays. *AIDS Research and Human Retroviruses*, *13*(9), 737–742. https://doi.org/10.1089/aid.1997.13.737

Romero, E. V., & Feder, A. F. (2024). Elevated HIV Viral Load is Associated with Higher Recombination Rate In Vivo. *Molecular Biology and Evolution*, *41*(1), msad260. https://doi.org/10.1093/molbev/msad260

Rosás-Umbert, M., Gunst, J. D., Pahus, M. H., Olesen, R., Schleimann, M., Denton, P. W., Ramos, V., Ward, A., Kinloch, N. N., Copertino, D. C., Escribà, T., Llano, A., Brumme, Z. L., Brad Jones, R., Mothe, B., Brander, C., Fox, J., Nussenzweig, M. C., Fidler, S., … Søgaard, O. S. (2022). Administration of broadly neutralizing anti-HIV-1 antibodies at ART initiation maintains long-term CD8+ T cell immunity. *Nature Communications*, *13*(1), 6473. https://doi.org/10.1038/s41467-022-34171-2

Saha, A., & Dixit, N. M. (2020). Pre-existing resistance in the latent reservoir can compromise VRC01 therapy during chronic HIV-1 infection. *PLOS Computational Biology*, *16*(11), e1008434. https://doi.org/10.1371/journal.pcbi.1008434

Sanders, R. W., Derking, R., Cupo, A., Julien, J.-P., Yasmeen, A., Val, N. de, Kim, H. J., Blattner, C., Peña, A. T. de la, Korzun, J., Golabek, M., Reyes, K. de los, Ketas, T. J., Gils, M. J. van, King, C. R., Wilson, I. A., Ward, A. B., Klasse, P. J., & Moore, J. P. (2013). A Next-Generation Cleaved, Soluble HIV-1 Env Trimer, BG505 SOSIP.664 gp140, Expresses Multiple Epitopes for Broadly Neutralizing but Not Non-Neutralizing Antibodies. *PLOS Pathogens*, *9*(9), e1003618. https://doi.org/10.1371/journal.ppat.1003618

Scheid, J. F., Horwitz, J. A., Bar-On, Y., Kreider, E. F., Lu, C.-L., Lorenzi, J. C. C., Feldmann, A., Braunschweig, M., Nogueira, L., Oliveira, T., Shimeliovich, I., Patel, R., Burke, L., Cohen, Y. Z., Hadrigan, S., Settler, A., Witmer-Pack, M., West, J., Juelg, B., … Caskey, M. (2016). HIV-1 antibody 3BNC117 suppresses viral rebound in humans during treatment interruption. *Nature*, *535*(7613), 556–560. https://doi.org/10.1038/nature18929

Schommers, P., Gruell, H., Abernathy, M. E., Tran, M.-K., Dingens, A. S., Gristick, H. B., Barnes, C. O., Schoofs, T., Schlotz, M., Vanshylla, K., Kreer, C., Weiland, D., Holtick, U., Scheid, C., Valter, M. M., van Gils, M. J., Sanders, R. W., Vehreschild, J. J., Cornely, O. A., … Klein, F. (2020). Restriction of HIV-1 Escape by a Highly Broad and Potent Neutralizing Antibody. *Cell*, *180*(3), 471-489.e22. https://doi.org/10.1016/j.cell.2020.01.010

Schoofs, T., Klein, F., Braunschweig, M., Kreider, E. F., Feldmann, A., Nogueira, L., Oliveira, T., Lorenzi, J. C. C., Parrish, E. H., Learn, G. H., West, A. P., Bjorkman, P. J., Schlesinger, S. J., Seaman, M. S., Czartoski, J., McElrath, M. J., Pfeifer, N., Hahn, B. H., Caskey, M., & Nussenzweig, M. C. (2016). HIV-1 therapy with monoclonal antibody 3BNC117 elicits host immune responses against HIV-1. *Science*, *352*(6288), 997–1001. https://doi.org/10.1126/science.aaf0972

Selzer, L., VanderVeen, L. A., Parvangada, A., Martin, R., Collins, S. E., Mehrotra, M., & Callebaut, C. (2025). Susceptibility Screening of HIV-1 Viruses to Broadly Neutralizing Antibodies, Teropavimab and Zinlirvimab, in People With HIV-1 Suppressed by Antiretroviral Therapy. *JAIDS Journal of Acquired Immune Deficiency Syndromes*, *98*(1), 64. https://doi.org/10.1097/QAI.0000000000003528

Sneller, M. C., Blazkova, J., Justement, J. S., Shi, V., Kennedy, B. D., Gittens, K., Tolstenko, J., McCormack, G., Whitehead, E. J., Schneck, R. F., Proschan, M. A., Benko, E., Kovacs, C., Oguz, C., Seaman, M. S., Caskey, M., Nussenzweig, M. C., Fauci, A. S., Moir, S., & Chun, T.-W. (2022). Combination anti-HIV antibodies provide sustained virological suppression. *Nature*, *606*(7913), 375–381. https://doi.org/10.1038/s41586-022-04797-9

Sohail, M. S., Louie, R. H. Y., McKay, M. R., & Barton, J. P. (2021). MPL resolves genetic linkage in fitness inference from complex evolutionary histories. *Nature Biotechnology*, *39*(4), 472–479. https://doi.org/10.1038/s41587-020-0737-3

Stephenson, K. E., Julg, B., Tan, C. S., Zash, R., Walsh, S. R., Rolle, C.-P., Monczor, A. N., Lupo, S., Gelderblom, H. C., Ansel, J. L., Kanjilal, D. G., Maxfield, L. F., Nkolola, J., Borducchi, E. N., Abbink, P., Liu, J., Peter, L., Chandrashekar, A., Nityanandam, R., … Barouch, D. H. (2021). Safety, pharmacokinetics and antiviral activity of PGT121, a broadly neutralizing monoclonal antibody against HIV-1: A randomized, placebo-controlled, phase 1 clinical trial. *Nature Medicine*, *27*(10), 1718–1724. https://doi.org/10.1038/s41591-021-01509-0

Swan, D. A., Rolland, M., Herbeck, J. T., Schiffer, J. T., & Reeves, D. B. (2022). Evolution during primary HIV infection does not require adaptive immune selection. *Proceedings of the National Academy of Sciences of the United States of America*, *119*(7), e2109172119. https://doi.org/10.1073/pnas.2109172119

Taiwo, B. O., Zheng, Y., Rodriguez, K., Burke, L., Reeves, J. D., Scarsi, K. K., Gama, L., Petropoulos, C. J., Belaunzaran-Zamudio, P. F., Wannamaker, P., D'Amico, R., Rathod, P., Bar, K. J., Tebas, P., & for the A5357 Study Team. (2025). Phase 2 Trial of Long-Acting Cabotegravir and VRC07-523LS for Viral Suppression in Adults With Human Immunodeficiency Virus Type 1: ACTG A5357. *Clinical Infectious Diseases*, ciaf375. https://doi.org/10.1093/cid/ciaf375

Tebas, P. (2025). Future of bNAbs in HIV Treatment. *Current HIV/AIDS Reports*, *22*(1), 34. https://doi.org/10.1007/s11904-025-00744-1

UNAIDS data 2024 | *UNAIDS*. (2024). Joint United Nations Programme on HIV/AIDS. https://www.unaids.org/en/resources/documents/2024/2024_unaids_data

Wagh, K., Bhattacharya, T., Williamson, C., Robles, A., Bayne, M., Garrity, J., Rist, M., Rademeyer, C., Yoon,

H., Lapedes, A., Gao, H., Greene, K., Louder, M. K., Kong, R., Karim, S. A., Burton, D. R., Barouch, D. H., Nussenzweig, M. C., Mascola, J. R., … Seaman, M. S. (2016). Optimal Combinations of Broadly Neutralizing Antibodies for Prevention and Treatment of HIV-1 Clade C Infection. *PLOS Pathogens*, *12*(3), e1005520. https://doi.org/10.1371/journal.ppat.1005520

Wain-Hobson, S., Sonigo, P., Danos, O., Cole, S., & Alizon, M. (1985). Nucleotide sequence of the AIDS virus, LAV. *Cell*, *40*(1), 9–17. https://doi.org/10.1016/0092-8674(85)90303-4

West, A. P., Scharf, L., Horwitz, J., Klein, F., Nussenzweig, M. C., & Bjorkman, P. J. (2013). Computational analysis of anti–HIV-1 antibody neutralization panel data to identify potential functional epitope residues. *Proceedings of the National Academy of Sciences*, *110*(26), 10598–10603. https://doi.org/10.1073/pnas.1309215110

Westfall, D. H., Deng, W., Pankow, A., Murrell, H., Chen, L., Zhao, H., Williamson, C., Rolland, M., Murrell, B., & Mullins, J. I. (2024). Optimized SMRT-UMI protocol produces highly accurate sequence datasets from diverse populations—Application to HIV-1 quasispecies. *Virus Evolution*, *10*(1), veae019. https://doi.org/10.1093/ve/veae019

Williams, K.-A., & Pennings, P. (2020). Drug Resistance Evolution in HIV in the Late 1990s: Hard Sweeps, Soft Sweeps, Clonal Interference and the Accumulation of Drug Resistance Mutations. *G3 (Bethesda, Md.)*, *10*(4), 1213–1223. https://doi.org/10.1534/g3.119.400772

Williamson, C., Moodley, C., Magaret, C. A., Giorgi, E. E., Rolland, M., Westfall, D. H., Yssel, A., Deng, W., Rossenkhan, R., Mkhize, N. N., Chen, L., Zhao, H., Bhattacharya, T., Pankow, A., Murrell, B., York, T., Gwashu-Nyangiwe, A., Ndabambi, N., Thebus, R., … Mullins, J. I. (2025). *Influence of the broadly neutralizing antibody VRC01 on HIV breakthrough virus populations in antibody-mediated prevention trials* (p. 2025.07.01.659979). bioRxiv. https://doi.org/10.1101/2025.07.01.659979

Wu, X., Parast, A. B., Richardson, B. A., Nduati, R., John-Stewart, G., Mbori-Ngacha, D., Rainwater, S. M. J., & Overbaugh, J. (2006). Neutralization Escape Variants of Human Immunodeficiency Virus Type 1 Are Transmitted from Mother to Infant. *Journal of Virology*, *80*(2), 835–844. https://doi.org/10.1128/jvi.80.2.835-844.2006

Yoon, H., Macke, J., West, A. P., Jr, Foley, B., Bjorkman, P. J., Korber, B., & Yusim, K. (2015). CATNAP: A tool to compile, analyze and tally neutralizing antibody panels. *Nucleic Acids Research*, *43*(W1),

W213–W219. https://doi.org/10.1093/nar/gkv404

Yu, T. C., Thornton, Z. T., Hannon, W. W., DeWitt, W. S., Radford, C. E., Matsen, F. A., IV, & Bloom, J. D. (2022). A biophysical model of viral escape from polyclonal antibodies. *Virus Evolution*, *8*(2), veac110. https://doi.org/10.1093/ve/veac110

Zacharopoulou, P., Lee, M., Oliveira, T., Thornhill, J., Robinson, N., Brown, H., Kinloch, S., Goulder, P., Fox, J., Fidler, S., Ansari, M. A., & Frater, J. (2024). Prevalence of resistance-associated viral variants to the HIV-specific broadly neutralising antibody 10-1074 in a UK bNAb-naïve population. *Frontiers in Immunology*, *15*. https://doi.org/10.3389/fimmu.2024.1352123

Zanini, F., Brodin, J., Thebo, L., Lanz, C., Bratt, G., Albert, J., & Neher, R. A. (2015). Population genomics of intrapatient HIV-1 evolution. *eLife*, *4*, e11282. https://doi.org/10.7554/eLife.11282

Zanini, F., Puller, V., Brodin, J., Albert, J., & Neher, R. A. (2017). In vivo mutation rates and the landscape of fitness costs of HIV-1. *Virus Evolution*, *3*(1), vex003. https://doi.org/10.1093/ve/vex003

Zhong, P., Peeters, M., Janssens, W., Fransen, K., Heyndrickx, L., Vanham, G., Willems, B., Piot, P., & Van Der Groen, G. (1995). Correlation between Genetic and Biological Properties of Biologically Cloned HIV Type 1 Viruses Representing Subtypes A, B, and D. *AIDS Research and Human Retroviruses*, *11*(2), 239–248. https://doi.org/10.1089/aid.1995.11.239

Zhou, T., Zhu, J., Wu, X., Moquin, S., Zhang, B., Acharya, P., Georgiev, I. S., Altae-Tran, H. R., Chuang, G.-Y., Joyce, M. G., Do Kwon, Y., Longo, N. S., Louder, M. K., Luongo, T., McKee, K., Schramm, C. A., Skinner, J., Yang, Y., Yang, Z., … Kwong, P. D. (2013). Multidonor Analysis Reveals Structural Elements, Genetic Determinants, and Maturation Pathway for HIV-1 Neutralization by VRC01-Class Antibodies. *Immunity*, *39*(2), 245–258. https://doi.org/10.1016/j.immuni.2013.04.012